Proposal for the J-PARC 50 GeV Proton Synchrotron

Direct measurement of the ${}^{3}_{\Lambda}$H and ${}^{4}_{\Lambda}$H lifetimes using the ^{3,4}He$(\pi^-, K^0)^{3,4}_{\Lambda}$H reactions

M. Agnello, S. Bufalino, G. Kaniadakis,
INFN - Sezione di Torino and
Politecnico di Torino, Department of Applied Science and Technology,
C.so Duca degli Abruzzi 24, 10129 Torino, Italy

E. Botta,
INFN - Sezione di Torino and University of Torino, Physics Department,
Via P. Giuria 1, 10125 Torino, Italy

T. Bressani, D. Calvo, A. Feliciello,
INFN - Sezione di Torino, Via P. Giuria 1, 10125 Torino, Italy

H. Tamura, Y. Ishikawa, A. Rogers,
Department of Physics, Tohoku University, Sendai 980-8578, Japan

T. Nagae,
Department of Physics, Kyoto University,
Kitashirakawa, Sakyo-ku, Kyoto, Japan

T. Takahashi, M. Ukai,
Institute of Particle and Nuclear Study (IPNS),
High Energy Accelerator Research Organization (KEK),
Oho 1-1, Tsukuba 305-0801, Japan

T.O. Yamamoto,
Advanced Science Research Center (ASRC),
Japan Atomic Energy Agency (JAEA),
Shirakata 2-4, Tokai, 319-1195, Japan

S. Ajimura, A. Sakaguchi,
Osaka University, Toyonaka, Osaka 560-0043, Japan

H. Outa
RIKEN, Wako, 351-0198, Japan

Executive summary

Some recent experimental determinations of ${}^{3}_{\Lambda}$H lifetime provided by three different heavy ion experiments (HypHI, STAR and ALICE) triggered a vivid debate. Contrarily to the expectations, the results seem to indicate the ${}^{3}_{\Lambda}$H lifetime is by far shorter than the one of the free Λ hyperon. However, the data are not in agreement with each other and they are affected by large errors.

The aim of this proposal is to perform for the first time a direct measurement of the ${}^{3}_{\Lambda}$H lifetime with a high accuracy. The described experimental setup could permit to measure as well the ${}^{4}_{\Lambda}$H lifetime and, possibly, to carry on a systematic study of the hypernucleus decay process for several Λ-hypernuclei belonging to the *p*-shell. Moreover, the measurement of the ${}^{4}_{\Lambda}$H nonmesonic decay width (Γ_p) will permit to test as well the validity of the ΔI = 1/2 rule.

In the following the most significant features of the project are listed:

physical process:	$\pi^- + {}^{3,4}\mathrm{He} \rightarrow K^0 \ + \ {}^{3,4}_{\Lambda}\mathrm{H}$
beam:	1.05 GeV/c π^-
beam line:	K1.1
beam intensity:	1×10^7 π^- / spill (5 s cycle operation)
beam request:	10 days for ${}^{4}_{\Lambda}$H study 30 days for ${}^{3}_{\Lambda}$H study
targets:	liquid ^{3}He liquid ^{4}He
detectors:	SKS complex coupled to a time of flight system, drift chambers and a range detector

Contents

1 Introduction **4**

2 Survey of the existing experimental data on $^{3}_{\Lambda}$H and $^{4}_{\Lambda}$H hypernuclei **6**

3 Overview of the theoretical predictions for $\tau(^{3}_{\Lambda}\mathrm{H})$ **11**

4 How to perform a precision measurement of the lifetime of the $^{3}_{\Lambda}$H and $^{4}_{\Lambda}$H hypernuclei **11**

5 The experimental approach to the (π^-,K^0) reaction on ^{3}He and ^{4}He at J-PARC **14**

5.1 The π^- beam and the π^+ spectrometers 18

5.2 The targets 20

5.3 The Time Of Flight measurement 20

5.4 The range scintillator detector 21

5.5 The trigger strategy 22

6 Monte Carlo simulations **23**

7 Expected apparatus performance **23**

8 $^{3}_{\Lambda}$H and $^{4}_{\Lambda}$H yields **26**

9 Momentum measurement and particle identification in the range detector **28**

10 Calibration of the apparatus **32**

11 Analysis of the data **33**

12 Expected backgrounds and their control **34**

13 Analysis of the time spectra **36**

A Possible measurement of the lifetime for medium to heavy neutron-rich Λ hypernuclei **38**

B Possible determination of the Nonmesonic Weak decay width Γ_p for $^{3}_{\Lambda}$H and $^{4}_{\Lambda}$H hypernuclei **43**

1 Introduction

The hypertriton ${}^{3}_{\Lambda}$H is the lowest mass Λ-hypernucleus. It is a very loosely bound baryonic system with total binding energy $B_{tot} = 2.35 \pm 0.05_{stat} \pm 0.04_{sys}$ MeV [1] ($B_{tot}/A = 0.784$ MeV/baryon). Moreover, it is the weakest bound known strange few-body baryonic system, since the separation energy of the Λ hyperon, B_Λ, is $0.13 \pm 0.05_{stat} \pm 0.04_{sys}$ MeV only [1].

It was observed at the beginning of the 60's by analyzing the events produced in the interaction of K^-, both in flight and at rest, with the nuclei of the sensitive layers of visualizing detectors (either photographic emulsions or He filled bubble chambers). The results obtained about ${}^{3}_{\Lambda}$H, particularly for the Λ binding energy B_Λ, were characterized by high precision, despite of the limited statistics of the data samples.

On the contrary, visualizing techniques permitted to determine only the gross features of the weak decay (WD) process. In the case of ${}^{3}_{\Lambda}$H the WD channels are essentially the mesonic ones (MWD):

$$ {}^{3}_{\Lambda}\mathrm{H} \rightarrow \pi^- + {}^{3}\mathrm{He} \ , \tag{1} $$
$$ {}^{3}_{\Lambda}\mathrm{H} \rightarrow \pi^0 + {}^{3}\mathrm{H} \ , \tag{2} $$
$$ {}^{3}_{\Lambda}\mathrm{H} \rightarrow \pi^- + d + p \ , \tag{3} $$
$$ {}^{3}_{\Lambda}\mathrm{H} \rightarrow \pi^0 + d + n \ , \tag{4} $$
$$ {}^{3}_{\Lambda}\mathrm{H} \rightarrow \pi^- + p + p + n \ , \tag{5} $$
$$ {}^{3}_{\Lambda}\mathrm{H} \rightarrow \pi^0 + p + n + n \ . \tag{6} $$

Indeed, the nonmesonic channels (NMWD) (${}^{3}_{\Lambda}\mathrm{H} \rightarrow d + n, \ p + n + n$) can be neglected as all theoretical estimates agree in setting their contribution to the total WD width (and then to the lifetime) to less than 2% [2].

Actually, the intrinsic experimental hardness to observe neutral particles and the limited statistics available played a crucial role in assessing the branching ratios of the different decay channels. For these reasons only the decay (1) was clearly observed and the ratio $R_3 = ({}^{3}_{\Lambda}\mathrm{H} \rightarrow \pi^- + {}^{3}\mathrm{He})/(\text{all } \pi^- \text{ MWD})$ was determined.

Even more problematic was the evaluation of the ${}^{3}_{\Lambda}$H lifetime. Since visualizing techniques do not allow direct time measurements, the determination of the lifetime $\tau({}^{3}_{\Lambda}\mathrm{H})$ was obtained from the spatial distribution of the π^- MWD vertices around the formation point of ${}^{3}_{\Lambda}$H. The maximum likelihood approach was usually adopted. The difficulty in disentangling events produced by K^- in flight or at rest resulted in large systematic errors which often added up to large statistical errors related to the very meagre samples of events. Thus, it was not possible to conclude if the reported values of $\tau({}^{3}_{\Lambda}\mathrm{H})$ were significantly different from the lifetime of the free Λ

($\tau(\Lambda_{\rm free}) = 263.2 \pm 0.2$ ps) [3]. The presumed equality $\tau({}^{3}_{\Lambda}{\rm H}) = \tau(\Lambda_{\rm free})$ seemed the plausible consequence of the hypothesis that the constituent Λ would spend most of its time far from the deuteron core due to the very small value of B_Λ. Several theoretical calculations also supported such a hypothesis.

Starting from the 70's, Hypernuclear Physics experiments adopted electronic techniques [4–8]. Thanks to the improvement of the intensity and of the quality of meson beams available worldwide, it became possible to produce, to select and to identify hypernuclei in their ground states by means of meson-induced, two-body reactions on nuclear targets. The reactions (K^-, π^-) at the BNL AGS and (π^+, K^+) at the KEK PS permitted to measure the lifetime of hypernuclei with direct timing techniques. Ref. [8] contains an updated overview and a summary of the obtained results. However, the technique could not be applied to the hydrogen hyperisotopes, ${}^{3}_{\Lambda}{\rm H}$ and ${}^{4}_{\Lambda}{\rm H}$, since the two-body reactions having an incoming charged meson and an outgoing charged meson require targets of radioactive ${}^{3}{\rm H}$, which are hard to deal with, or of ${}^{4}{\rm H}$, which does not exist. The unclear situation of $\tau({}^{3}_{\Lambda}{\rm H})$ was then practically forgotten.

Suddenly, the interest in the experimental value of $\tau({}^{3}_{\Lambda}{\rm H})$ has grown again in the last few years, triggered by surprising results from experiments studying central ultrarelativistic Heavy Ions collisions (urHIc), STAR at BNL RHIC and ALICE at CERN LHC, or relativistic ion fragmentation, HypHI at GSI SIS. Even though generally affected by large statistical and systematic errors, the values reported by these three experiments reopen the question about the statement that $\tau({}^{3}_{\Lambda}{\rm H})$ is close to $\tau(\Lambda_{\rm free})$.

In the case of ${}^{4}_{\Lambda}{\rm H}$ the WD channels are primarily the MWD ones:

$$
\begin{aligned}
{}^{4}_{\Lambda}{\rm H} &\to \pi^- + {}^{4}{\rm He} \ , && (7)\\
{}^{4}_{\Lambda}{\rm H} &\to \pi^- + n + {}^{3}{\rm He} \ , && (8)\\
{}^{4}_{\Lambda}{\rm H} &\to \pi^- + p + {}^{3}{\rm H} \ , && (9)\\
{}^{4}_{\Lambda}{\rm H} &\to \pi^- + d + d \ , && (10)\\
{}^{4}_{\Lambda}{\rm H} &\to \pi^0 + t + n \ , && (11)\\
{}^{4}_{\Lambda}{\rm H} &\to \pi^0 + d + n + n \ , && (12)\\
{}^{4}_{\Lambda}{\rm H} &\to \pi^0 + p + n + n + n \ . && (13)
\end{aligned}
$$

The NMWD channels (${}^{4}_{\Lambda}{\rm H} \to d+n+n,\ p+n+n+n$) should have a branching ratio of $\approx 18\%$ following old evaluations which date back to the early '60s [9].

More clear is the status of the experimental values reported for the lifetime of ${}^{4}_{\Lambda}{\rm H}$, $\tau({}^{4}_{\Lambda}{\rm H})$. Old measurements performed with emulsions reported results affected by very large errors. Subsequent results by experiments with

counters, carried out with K^- in flight at the BNL AGS, with K^- at rest at the KEK PS and with relativistic ion fragmentation at the Dubna Synchrophasotron and at GSI SIS, indicated that $\tau(^4_\Lambda\mathrm{H})$ is lower than $\tau(\Lambda_{\mathrm{free}})$. This fact can be qualitatively understood taking into account that $\mathrm{B}(^4_\Lambda\mathrm{H})$ $= 2.157 \pm 0.005_{\mathrm{stat}} \pm 0.077_{\mathrm{sys}}$ MeV [10]. Moreover, very interesting is the comparison with the lifetime of the hyperisobar $^4_\Lambda$He (250 $\pm$ 18 ps) [8], which on the contrary is significantly longer than the lifetime of $^4_\Lambda$H.

From the above considerations, it is evident that it is highly desirable that a dedicated experiment on the lifetime of the hydrogen hyperisotopes is performed in the near future, using the well known method of time delay spectra and with a precision better than 10%.

2 Survey of the existing experimental data on $^3_\Lambda$H and $^4_\Lambda$H hypernuclei

Table 1 reports the chronology of the measurements existing for the lifetime of $^3_\Lambda$H. The laboratory, the beam, the experimental method, the value of the lifetime with the error (statistical and systematic when available) and the Reference are listed.

A critical review of the experimental data available until 2016 was recently carried out in Ref. [26]. As it was already pointed out, all the measurements performed with visualizing techniques produced meagre samples of events, sometimes less than 10. The inferred values of $\tau(^3_\Lambda\mathrm{H})$ were consequently affected by very large errors, often exceeding 100%, and it was not possible to draw any firm conclusion about their comparison with $\tau(\Lambda_{\mathrm{free}})$. Anyway, from the data set of Table 1, it is possible to deduce different weighted averages (w.a.) for $\tau(^3_\Lambda\mathrm{H})$. We use the method described in Ref. [27] to take into account asymmetric errors. For the emulsion data series we obtain a w.a. of 203^{+40}_{-31} ps, for the He Bubble Chamber one a w.a. of 193^{+15}_{-13} ps and for the data sample of both the visualizing techniques a w.a. of 195^{+14}_{-13} ps. A substantial consistency then exists among the w.a. values of the data sets obtained with visualizing techniques.

The precision of the measurements improved significantly, thanks to the first results provided by experiments studying (heavy) ion collisions. In particular, the three values provided by STAR, HypHI and ALICE [20, 22, 23] were in nice agreement to each other and they seemed to indicate that $\tau(^3_\Lambda\mathrm{H})$ was of the order of 70% of $\tau(\Lambda_{\mathrm{free}})$: actually their w.a. turned out to be 182^{+28}_{-23} ps. In this respect, it is worth to remind that the value published in Ref. [21] is still labeled as preliminary and it was then not taken into account.

Table 1: Chronology of ${}^{3}_{\Lambda}$H lifetime measurements: year, laboratory, beam, experimental technique, measured lifetime and publication Reference are given. rHIc stands for relativistic heavy-ions collisions, urHIc for ultra relativistic heavy-ions collisions. (Updated from Ref. [26])

year	laboratory	beam	exp. technique	lifetime (ps)	Reference
1963	LBL Bevatron	stopped K^-	He bubble chamber	105^{+20}_{-18}	[9]
1964	BNL AGS	K^-, 2.3-2.5 GeV/c	ph. emulsion	90^{+220}_{-40}	[11]
1965	BNL AGS and LBL Bevatron	K^-, 2.3 GeV/c K^-, 790 MeV/c	ph. emulsion	340^{+820}_{-140}	[12]
1968	ANL ZGS	stopped K^-	He bubble chamber	232^{+45}_{-34}	[13]
1968	LBL Bevatron	K^-, 1.1 GeV/c	ph. emulsion	274^{+110}_{-72}	[14]
1969	BNL AGS	K^-, 1.1 GeV/c	ph. emulsion	285^{+127}_{-105}	[15]
1970	CERN PS	stopped K^-	ph. emulsion	128^{+35}_{-26}	[16]
1970	ANL ZGS	stopped K^-	He bubble chamber	264^{+84}_{-52}	[17]
1973	ANL ZGS	stopped K^-	He bubble chamber	246^{+62}_{-41}	[18]
1992	Dubna Synchrophasotron	He, Li ions 2.2-5 AGeV rHIc	counter experiment	240^{+170}_{-100}	[19]
2010	BNL RHIC	Au-Au $\sqrt{s_{NN}}$=200 GeV central urHIc	counter experiment	$182^{+89}_{-45} \pm 27$	[20]
2013	BNL RHIC	Au-Au $\sqrt{s_{NN}}$=7.7-200 GeV central urHIc	counter experiment	$123^{+26}_{-22} \pm 10$	[21]
2013	GSI SIS	Li ions 2 AGeV peripheral rHIc	counter experiment	$183^{+42}_{-32} \pm 37$	[22]
2016	CERN LHC	Pb-Pb $\sqrt{s_{NN}}$=2.76 TeV central urHIc	counter experiment	$181^{+54}_{-38} \pm 33$	[23]
2017	BNL RHIC	Au-Au $\sqrt{s_{NN}}$=200 GeV central urHIc	counter experiment	$155^{+25}_{-22} \pm 31$	[24]
2018	BNL RHIC	Au-Au $\sqrt{s_{NN}}$=200 GeV central urHIc	counter experiment	$142^{+24}_{-21} \pm 31$	[25]

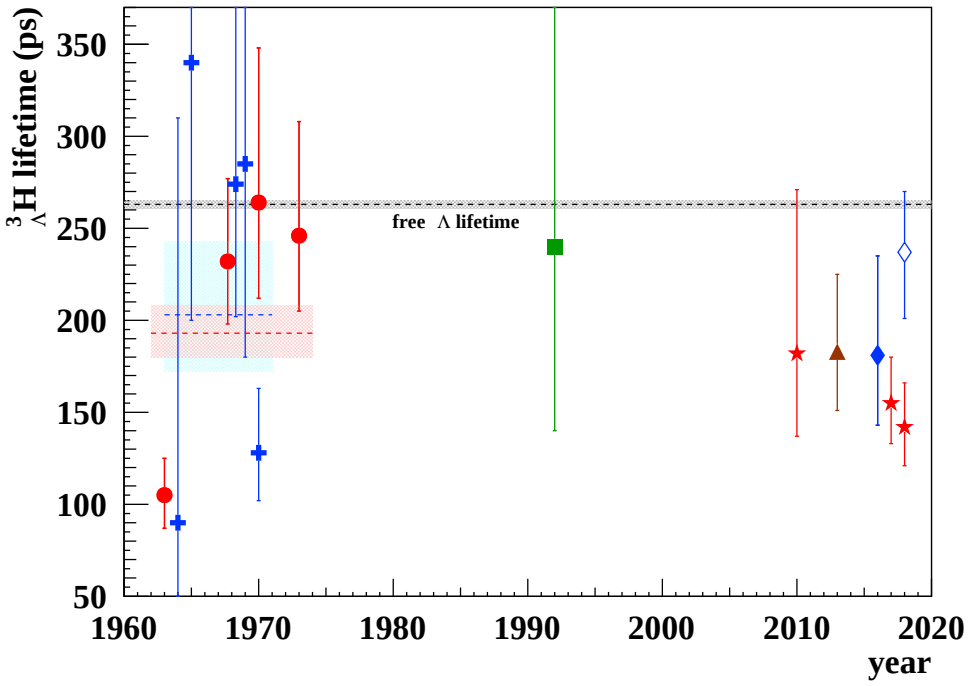

Figure 1: Chronological synopsis of the experimental data on $^{3}_{\Lambda}$H lifetime: red circles indicate results from He bubble chambers [9, 13, 17, 18], blue crosses results from photographic emulsions [11, 12, 14–16], green square result from Dubna counter experiment [19], red stars results from STAR experiment [20, 24, 25], brown upward triangle result from HypHI [22] and blue solid diamond result from ALICE [23]. The blue open diamond is the latest, still unpublished, ALICE determination. Colored dashed lines and hatched areas represent the corresponding w.a.′s and errors. (Updated from Ref. [26])

The puzzle was further fed by the last two recent determinations by the STAR Collaboration [24, 25] which reduced more and more the value of the measured $\tau(^{3}_{\Lambda}\mathrm{H})$. The w.a. of the values published by all the experiments based on electronic techniques (Refs. [19, 20, 22–25]) is 163^{+11}_{-10} ps. When one neglects the old measurement performed at the Dubna Synchrophasotron [19], the results from the STAR, the HypHI and the ALICE experiments led now to a w.a. $= 161^{+12}_{-10}$ ps.

Of completely opposite sign is the latest, but still unpublished, result announced by the ALICE Collaboration during the HADRON 2017, the Quark Matter 2018 and the HYP 2018 Conferences. A refined analysis of the latest

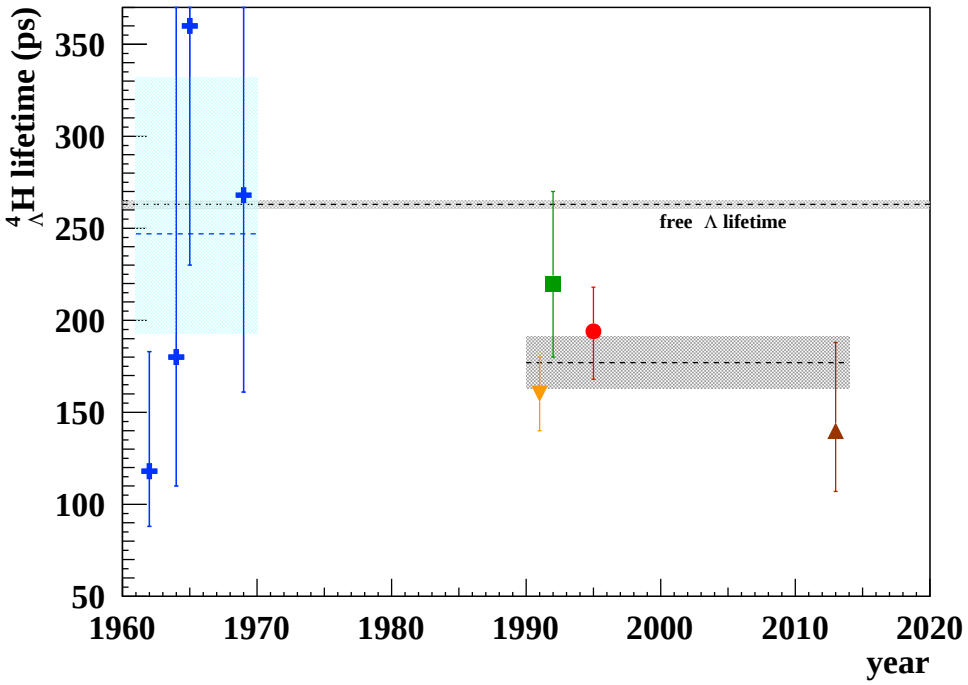

Figure 2: Chronological synopsis of the experimental data on ${}^{4}_{\Lambda}$H lifetime: blue crosses indicate results from photographic emulsions [11,12,15,28], while orange downward triangle [29], green square [19], red dot [30] and brown upward triangle [22] indicate results from counter experiments. Colored dashed lines and hatched areas represent the corresponding w.a.′s and errors. (Adapted from Ref. [26])

data sample collected at $\sqrt{s_{\rm NN}} = 5.02$ TeV led to a value for $\tau({}^{3}_{\Lambda}{\rm H})$ fully compatible with $\tau(\Lambda_{\rm free})$. If confirmed, such a result is no longer in agreement with the STAR claim, even within the error, and it makes difficult the comparison among the data coming from (heavy) ion physics. Fig. 1 shows the overview of the available experimental points.

This puzzling situation clearly requires a dedicated, well focused experiment in order to measure the $\tau({}^{3}_{\Lambda}{\rm H})$, relying on direct time measurement techniques, with a precision better than 10%, possibly 5%.

Table 2 reports the chronology of the experimental data existing for the lifetime of ${}^{4}_{\Lambda}$H, with the same format of Table 1. The first data, obtained from the analysis of events recorded by emulsions exposed to K^- beams, suffered from meagre statistics and consequently they were affected by huge errors. Better results were obtained in the following years by experiments

Table 2: Chronology of ${}^{4}_{\Lambda}$H lifetime measurements: laboratory, beam, experimental technique, measured lifetime and publication reference are given. rHIc stands for relativistic heavy-ions collisions. (from Ref. [26])

year	laboratory	beam	exp. technique	lifetime (ps)	reference
1962	LBL Bevatron	K^- 800 MeV/c	ph. emulsion	118^{+65}_{-30}	[28]
1964	BNL AGS	K^-, 2.3-2.5 GeV/c	ph. emulsion	180^{+250}_{-70}	[11]
1965	BNL AGS and LBL Bevatron	K^-, 2.3 GeV/c K^-, 790 MeV/c	ph. emulsions	360^{+490}_{-130}	[12]
1969	BNL AGS	K^-, 1.1 GeV/c	ph. emulsions	268^{+166}_{-107}	[15]
1991	BNL AGS	K^-, 800 MeV/c	counter experiment	160 ± 20	[29]
1992	Dubna Synchrophasotron	He, Li ions 2.2-5 AGeV rHIc	counter experiment	220^{+50}_{-40}	[19]
1995	KEK PS	stopped K^-	counter experiment	194^{+24}_{-26}	[30]
2013	GSI SIS	Li ions 2 AGeV peripheral rHIc	counter experiment	140^{+48}_{-33}	[22]

with electronic techniques studying reactions induced by K^- or by relativistic light ions. Production of neither ${}^{4}_{\Lambda}\mathrm{H}$ nor ${}^{\overline{4}}_{\overline{\Lambda}}\overline{\mathrm{H}}$ was observed in central urHIc, as expected on the basis of model predictions which indicate yields by 2 to 3 orders of magnitudes lower than those for ${}^{3}_{\Lambda}\mathrm{H}$ and ${}^{\overline{3}}_{\overline{\Lambda}}\overline{\mathrm{H}}$ [31]. From the emulsions data set we deduce for $\tau({}^{4}_{\Lambda}\mathrm{H})$ a w.a. value of 247^{+85}_{-54} ps and from the electronic counter experiment results a value of 177^{+14}_{-14} ps. The w.a. of all the data is 183^{+13}_{-13} ps with a reduced χ^2 of 1.68. Fig. 2 shows the overview of the available data for each experimental method and the w.a. values discussed above.

In conclusion the present data give a strong indication that $\tau({}^{4}_{\Lambda}\mathrm{H})$ is lower than $\tau(\Lambda_{\mathrm{free}})$. This is not surprising if one takes into account the present theoretical speculations on the subject. However, a new measurement with the time delay spectra technique with a precision better than 5% will be very useful for the quantitative comparison with the theoretical evaluations.

3 Overview of the theoretical predictions for $\tau({}^{3}_{\Lambda}\mathrm{H})$

Since the beginning, significant efforts were put in place in order to evaluate the $\tau({}^{3}_{\Lambda}\mathrm{H})$. The most recent evaluation of $\tau({}^{3}_{\Lambda}\mathrm{H})$ was done by Kamada and collaborators [2]. The MWD of the hypertriton was calculated by adopting rigorous solutions of three-body Faddeev equations for the hypernucleus wave function and for the $3N$ scattering states, in which realistic NN and YN interactions were used. The total MWD rate was found to be 101% of the free Λ-decay rate. By adding a 1.7% contribution from the total NMWD rate, a value of 256 ps was finally predicted for $\tau({}^{3}_{\Lambda}\mathrm{H})$, which seems to confirm the naive expectation that the lifetime of the hypertriton is very close to that for the free Λ.

Fig. 3 shows the results obtained by different author in several works about $\tau({}^{3}_{\Lambda}\mathrm{H})$ by following very different approaches. A complete discussion on these aspects can be found in Ref. [26].

4 How to perform a precision measurement of the lifetime of the ${}^{3}_{\Lambda}\mathrm{H}$ and ${}^{4}_{\Lambda}\mathrm{H}$ hypernuclei

The most reliable method for measuring the lifetime of hypernuclei in counter experiment is in principle very simple. The hypernucleus under study must

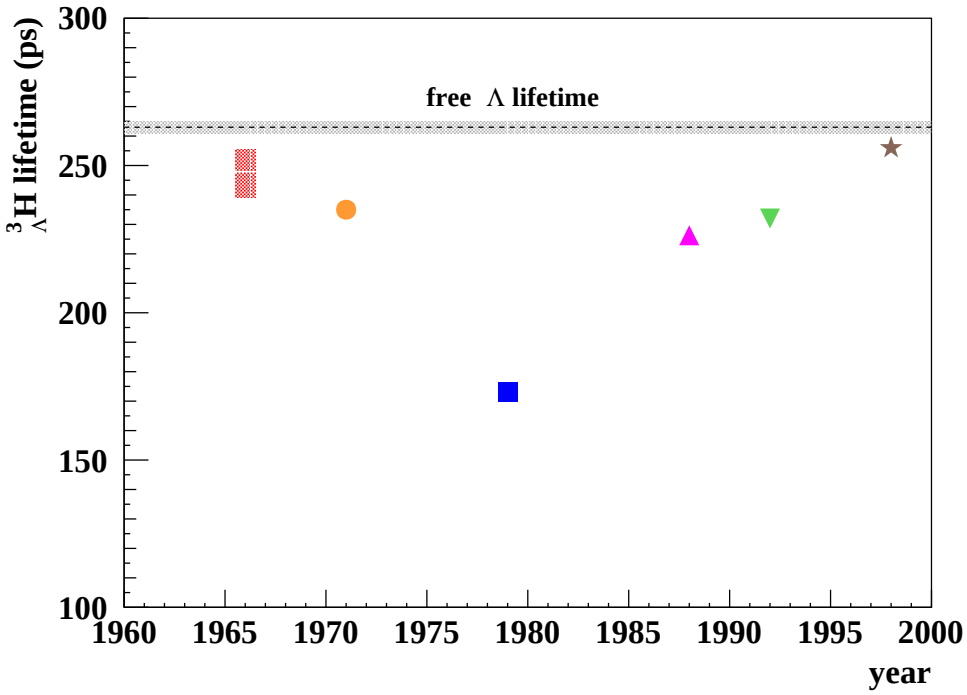

Figure 3: Chronological synopsis of the theoretical evaluations of $^{3}_{\Lambda}$H lifetime. The red hatched area represents the $\tau(^{3}_{\Lambda}\mathrm{H})$ range evaluated in Ref. [32], while the orange dot, the blue square, the magenta upward triangle, the green downward triangle and the brown star are the outcome of Refs. [33], [34], [35], [36] and [2], respectively. (Adapted from Ref. [26])

be selected and identified with a magnetic spectrometer featuring the best achievable resolution on the missing mass (MM) of the studied reaction. The time distribution of the charged particles emitted in the WD (essentially pions in the case of $^{3}_{\Lambda}$H and $^{4}_{\Lambda}$H) must be measured with a resolution better than 100 ps (rms). A fit of the time distribution to an exponential decay function broadened by the instrumental time resolution function provides the lifetime. If the time delay spectra is substantially background-free, the error on the lifetime turns out to be roughly equivalent to the statistical error on the number of events contained in the spectrum, as shown by the available literature [8].

The largest part of the experimental investigation in Hypernuclear Physics exploiting counter techniques was carried out by using two-body reactions. Chronologically, they were: (K^-, π^-) in flight or at rest, (π^+, K^+) in flight and $(e, e'K^+)$, or more precisely (γ^*, K^+), on a nuclear target ^{A}Z. With the

first two reactions the hypernucleus ${}^{A}_{\Lambda}$Z was produced, with the third the hypernucleus ${}^{A}_{\Lambda}$(Z-1). A detailed account of the properties of these reactions can be found in Refs. [4, 6, 7].

The electroproduction reaction $(e, e'K^+)$ can be exploited to produce ${}^{3}_{\Lambda}$H and ${}^{4}_{\Lambda}$H hypernuclei by using targets of ^{3}He and ^{4}He. Actually, a first study, performed with a spectrometer system featuring a final MM resolution of ≈ 4 MeV (FWHM), clearly showed signals corresponding to the production of ${}^{3}_{\Lambda}$H and ${}^{4}_{\Lambda}$H [37] and the corresponding cross sections were determined. More recently, a proposal was approved for a series of studies of the ΛN interactions in which cryogenic gaseous ^{3}He and ^{4}He targets could be used [38]. A preliminary study was done [39] in order to evaluate whether the approved setup (targets and magnetic spectrometers featuring a MM resolution of about 500 keV (FWHM)) could be used to determine the lifetimes, thanks to an additional detector system to identify the π^- from the MWD of the hydrogen hyperisotopes. Beam times up to 100 days were deduced. More realistic beam times were foreseen by using instead liquid targets, but there is a warning on the severe electromagnetic background that could affect the π^- detector system which have to be installed very close to the production target. In conclusion, a measurement of the lifetimes of ${}^{3}_{\Lambda}$H and ${}^{4}_{\Lambda}$H seems not feasible at JLab, at least in the short term.

Other two-body reactions that may be exploited to produce ${}^{3}_{\Lambda}$H and ${}^{4}_{\Lambda}$H from targets of ^{3}He and ^{4}He are:

$$\begin{array}{rcl} K^- + {}^{3,4}\mathrm{He} & \rightarrow & \pi^0 \; + \; {}^{3,4}_{\Lambda}\mathrm{H} \\ & & \hookrightarrow \gamma\gamma \end{array} \tag{14}$$

with K^- in flight or at rest, and

$$\begin{array}{rcl} \pi^- + {}^{3,4}\mathrm{He} & \rightarrow & K^0 \; + \; {}^{3,4}_{\Lambda}\mathrm{H} \\ & & \hookrightarrow \pi^+\pi^- \end{array} \tag{15}$$

using π^- with momentum in the range (1.0-1.1) GeV/c.

Excellent K^- and π^- beams are now available at J-PARC and the dynamics of reactions (14) and (15) is quite well known since their isospin conjugated (K^-, π^-) and (π^+, K^+) reactions on nuclei were used for over than four decades to produce the bulk of Hypernuclear Physics data and in particular to study WD processes. The main experimental difficulty intrinsic in reactions (14) and (15) is the precise determination of the π^0 or of the K^0 momentum vector, respectively. Indeed, a MM resolution on the order of 3 MeV (FWHM) is required to allow the separation of the ${}^{4}_{\Lambda}$H ground state from the Λ quasi free production background. Finally, it is important to note

that reaction (15) is well established and it has the experimental advantage of requiring the detection of charged particle only to be completely measured.

Just for fixing some numbers, the kinetic energy of the neutral meson must be determined to better than 3 MeV (FWHM) and its direction within 100 mrad (FWHM). However, the same resolution would not be equally effective for the loosely bound ${}^{3}_{\Lambda}$H.

Up to now, no high resolution K^0 spectrometer was used in experiments with nuclear targets. The technology of setting up two magnetic devices to detect both charged pions emitted in the K^0 decay is well known, but human and capital costs are high and the time scale for preparation would be long. However, the short term plan for the approved physics program at the J-PARC Experimental Hadron Facility (HEF) offers a unique opportunity for realizing a spectrometer for K^0 with high MM resolution that could be used for a series of new experiments in Hypernuclear Physics, which would include the measurement of ${}^{3}_{\Lambda}$H and ${}^{4}_{\Lambda}$H lifetime.

5 The experimental approach to the (π^-, K^0) reaction on ^{3}He and ^{4}He at J-PARC

The SKS magnetic spectrometer has been moved from the K1.8 beam line of the J-PARC HEF to the recently created K1.1 beam area. Fig. 4 shows a sketch of the new arrangement [40]. It is worth to remind that the SKS spectrometer features a solid angle acceptance of ≈ 100 msr and that a total MM resolution better than 1.5 MeV (FWHM) was obtained in the study of the (π^+, K^+) reaction on a thin Carbon target at 1.05 GeV/c [41]. The typical momentum of the outgoing K^+ for the (π^+, K^+) reaction is around 700 MeV/c.

These figures of merit have been kept in mind in evaluating a possible upgrade of such an experimental setup aiming to high resolution MM spectroscopy of the (π^-, K^0) reaction on nuclear targets. Actually, the idea is to study reaction (15) on liquid ^{3}He and ^{4}He, by measuring the momentum vectors of the $\pi^+\pi^-$ pairs following the K^0_S decay (BR $= 0.6920 \pm 0.0005$ [3]). The best choice is to measure π^+ with the SKS because, this way, the transmitted π^- beam is swept away and the parasitic interactions in the magnet yoke are minimized. Fig. 5 shows the outcome of a phase space simulation of reaction (15) at 1.05 GeV/c, obtained by using the GENBOD package. The upper panel shows the distribution of the momentum of the π^- versus the momentum of the π^+ for ${}^{4}_{\Lambda}$H production, when the π^+ is detected in the forward angular range (2°-14°) with respect to the incoming beam direction and

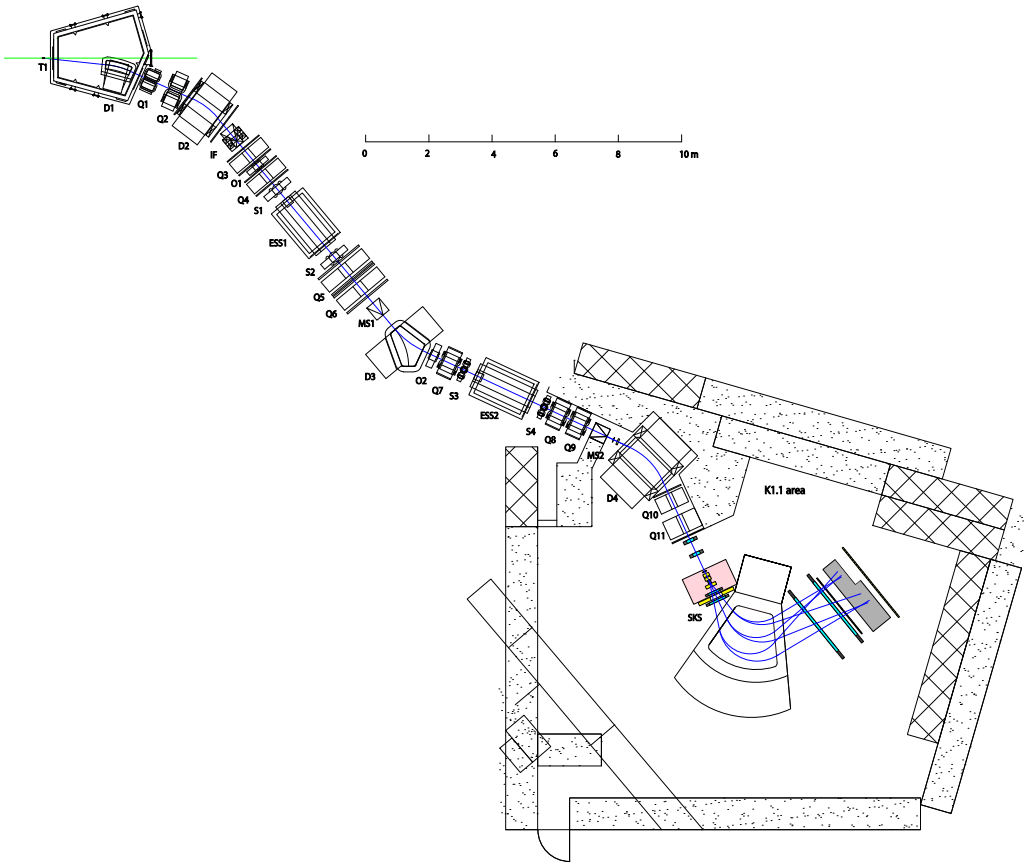

Figure 4: Layout of the J-PARC K1.1 beam line and K1.1 experimental area. From Ref. [40]

.

a momentum $\geq$ 650 MeV/c is chosen to match the SKS acceptance. Such constraints select a K^0_S emitted in the range (0°-22°). The middle panel of Fig. 5 shows the correlation between the π^+ and π^- angles and the lower panel shows the correlation between the decay π^- momentum and its angle.

In order to reach a MM resolution better than 3 MeV (FWHM) for reaction (15) by using the determination of the π^+ momentum measured with the SKS, it is necessary to have a good beam momentum measurement ($\Delta p/p \approx 10^{-4}$) and to detect the π^- vector momentum with a resolution better 2 MeV/c (FWHM) (see Section 7), an angular resolution better than 100 mrad (FWHM) and over a total solid angle as large as possible for all charged particles produced in process (15) and following the produced Λ-hypernucleus decay. Negative pion energies lower than 45 MeV should be

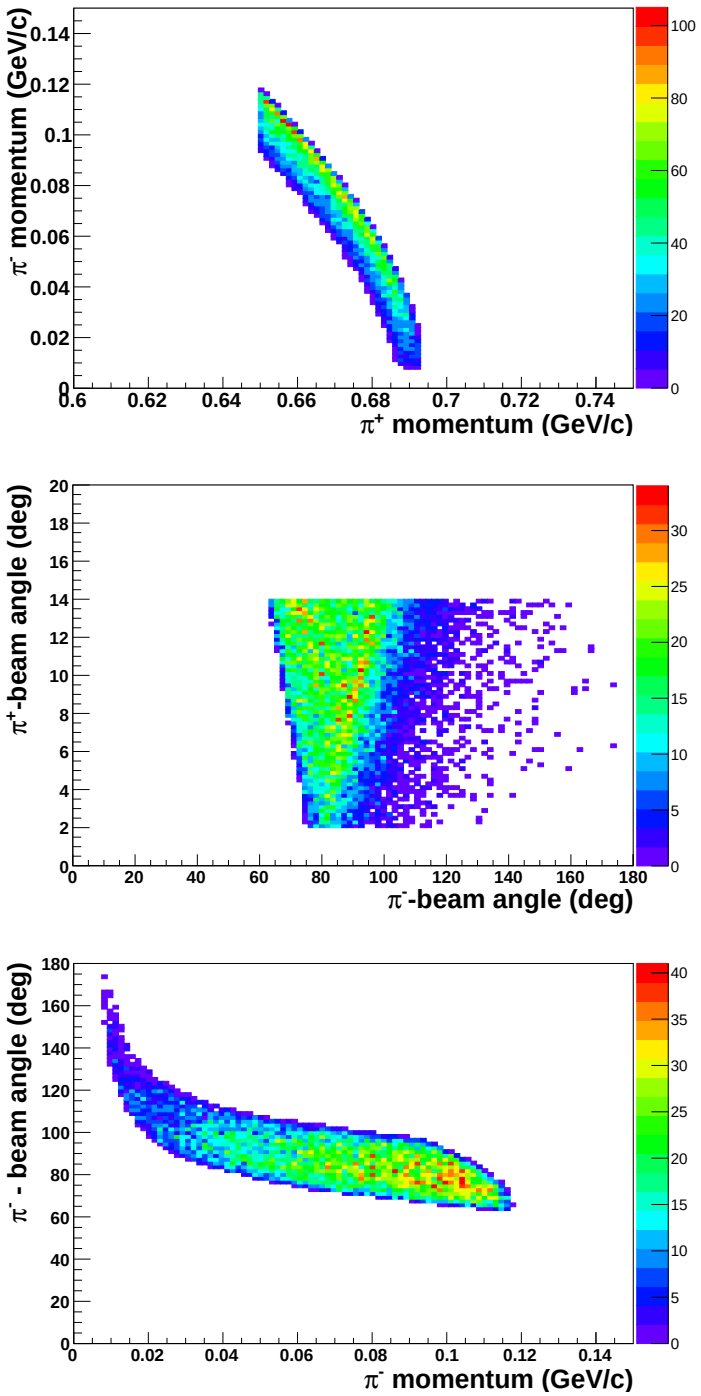

Figure 5: Phase-space simulation of the $\pi^- + {}^4\mathrm{He} \rightarrow K^0 + {}^4_\Lambda\mathrm{H} \rightarrow (\pi^+\pi^-) + {}^4_\Lambda\mathrm{H}$ reaction at 1.05 GeV/c in the SKS angular ($2^\circ < \theta_{\pi^+-beam} < 14^\circ$) and momentum ($p_{\pi^+} \geq 650$ MeV/c) acceptance. Upper panel: (π^+, π^-) momentum correlation, middle panel: (π^+, π^-) angular correlation, lower panel: K^0 decay π^- angle-momentum correlation.

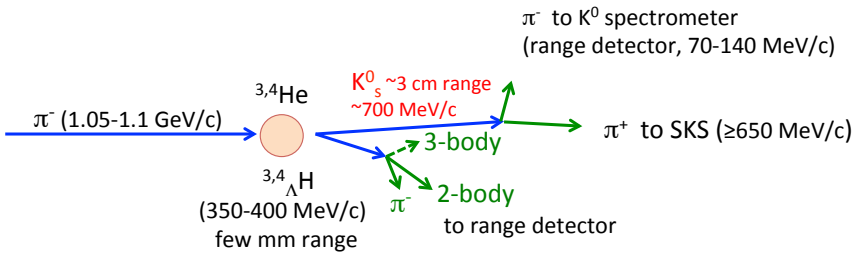

Figure 6: Schematic representation of the kinematical features of the reaction chain (15), followed by the ${}^{3}_{\Lambda}$H or ${}^{4}_{\Lambda}$H two- or three-body MWD that could be detected by using the SKS spectrometer coupled to the range scintillator hodoscope system.

covered; these correspond to momenta lower than 120 MeV/c. This is the same range of interest for π^- from the MWD of ${}^{3}_{\Lambda}$H and ${}^{4}_{\Lambda}$H. A modular, fine-grained range scintillator hodoscope seems the most adequate detector able to attain the desired performance for the energy determination. A pair of planar low-mass x-y drift chambers, spaced by some cm and with a spatial resolution ≈ 250 μm (FWHM) should allow the determination of the direction of the π^- to better than 100 mrad (FWHM). They should be able to sustain a flux of charged particles ranging from some tens to some hundreds $(\mathrm{s{\cdot}cm^2})^{-1}$ (see Section 12).

Fig. 6 gives a schematic view of the kinematic and of the topological features of the reaction chain (15), followed by the ${}^{3}_{\Lambda}$H or ${}^{4}_{\Lambda}$H two- or three-body MWD, that could be studied by using the SKS spectrometer together with the range scintillator hodoscope system surrounding the target: strongly asymmetric configurations of the K^0_S decay can be selected to tag the hypernucleus formation and decay. Fig. 7 shows a pictorial view of the proposed *target-range hodoscope region* experimental set-up, as it is currently implemented in the GEANT4 simulation program: it is composed by the liquid He target and related vacuum system structure (CFRP), a scintillator barrel for measuring the hypernucleus decay time, pairs of drift chambers in front of the range hodoscope modules to measure the particles direction and to allow the momentum determination and the particle identification. All components have been carefully simulated by means of the Geant4 toolkit [42] and optimized to fulfill the requirements. They will be described in the following.

Finally, Fig. 8 gives a scheme of the integration of the *target-range ho-*

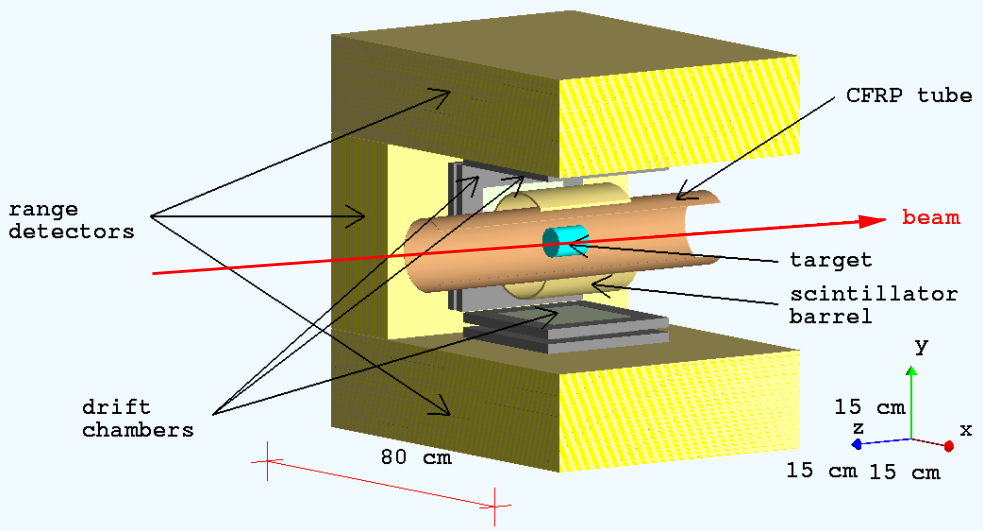

Figure 7: Pictorial view of the proposed *target-range hodoscope region* experimental set-up, as it is currently implemented in the GEANT4 simulation program. One of the quadrant of the apparatus has been removed to permit to see the interior details.

doscope region set-up with the SKS spectrometer.

As described in Appendix A, the reaction (π^-,K^0) can be exploited also to carry on a systematic study of the hypernucleus decay process for several Λ-hypernuclei belonging to the p-shell. Another important topic that can be addressed with the reaction (π^-,K^0) is the measurement of the ${}^{4}_{\Lambda}$H NMWD width (Γ_p) which will permit to test the validity of the ΔI $= 1/2$ rule, as discussed in Appendix B.

5.1 The π^- beam and the π^+ spectrometers

On the basis of the available information, it is estimated that K1.1 beam line spectrometer will feature a momentum resolution $\Delta p/p \approx 2 \times 10^{-3}$. The actual performance of the K1.1 beam line spectrometer will be confirmed by E63, a preceding experiment that will run at the K1.1 beam line, which uses almost the same setup for the beam line and the SKS spectrometers.

The beam timing for the lifetime measurement will be given by a scintillator hodoscope located on the beam in front of the target. Due to the high beam intensity, it will consist of two layers of plastic scintillators of size $\approx 10[L] \times 10[W] \times 1.5[T]$ cm^3, each segmented in 4 tiles with smaller width for the two central (1.3-1.5 cm) and larger (3.5-3.7 cm) for the two lateral

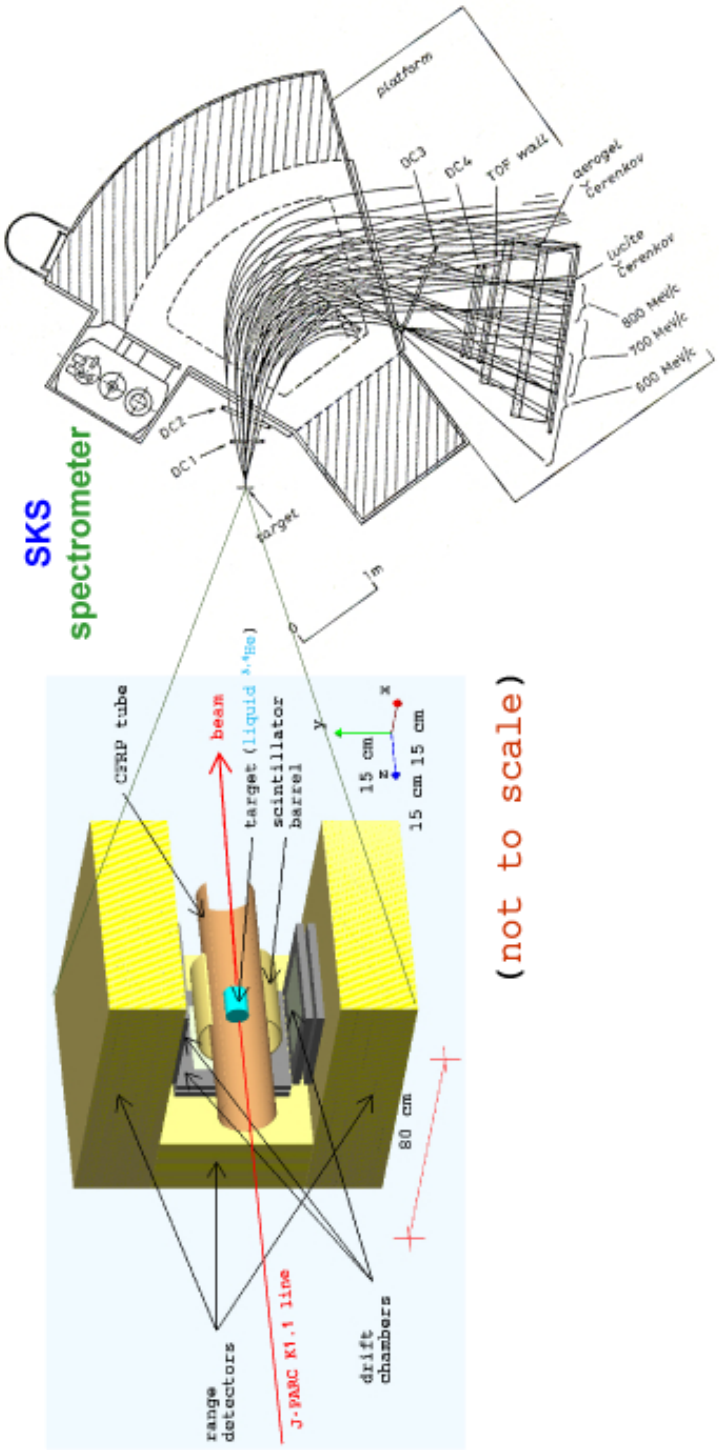

Figure 8: Conceptual scheme of the proposed integration of the *target-range hodoscope assembly* and of the SKS spectrometer. One of the quadrant of the apparatus has been removed to permit to see the interior details.

ones. Each tile will be read at both ends by photomultipliers with suitable electronics to avoid nonlinearity effects at high beam rates. The hodoscope is redundant to take into account the known saturation of the time resolution improvement with the number of scintillation photons [45]: during the data analysis procedure, the beam timing could be obtained by averaging the timings of the two layers.

5.2 The targets

The targets of liquid ^{3}He and ^{4}He will be manufactured under the supervision of the KEK experts. For this reason, we quote at the moment approximate dimensions only. We foresee a radius of 2-3 cm and a length of 7-10 cm. The final dimensions should also take into account the available amount of liquid ^{3}He and its cost. In the following we assume a radius of 3.0 cm and a length of 10.0 cm, equivalent to a thickness of 0.8 g/cm^2 in the case of the liquid ^{3}He target and, respectively, of 1.25 g/cm^2 in the case of the liquid ^{4}He one.

5.3 The Time Of Flight measurement

While the present uncertainty on the target assembly prevents the definition of the surrounding scintillator barrel radius, as far as its length it concerned it should be three times the longitudinal extension of the liquid ^{3}He or ^{4}He volume. This will ensure an optimal solid angle coverage for the time of flight (ToF) measurement of the prongs following the ${}^3_\Lambda$H decay processes (1) and (3) and the analogous ${}^4_\Lambda$H decay channels (7)-(10). Its thickness will be 0.5 cm, suited also for π and p identification.

However, it is possible to fix all the experimental and technical details needed to achieve a time resolution better than 100 ps (rms), that should remain stable over the whole data taking period (some weeks in the case of the ^{3}He target). To this purpose, we will exploit the know-how acquired during the latest measurements carried out by the SKS Collaboration at KEK, by the OBELIX Collaboration at CERN and by the FINUDA Collaboration at LNF.

The ToF barrel will consist of 30 scintillator staves, viewed at both ends by fast photomultipliers (PMs). The final transverse dimension of the slabs will be chosen according to the geometrical characteristics of the coupled PMs. This does not affect the following considerations:

- the signals should be sent to constant fraction discriminator modules (CFD), featuring the best performance for ToF measurement. A mean

timer (MT) should be obtained from each slab for fast coincidence to be implemented in the trigger strategy (based on hit multiplicity);

- a careful time alignment of the scintillator slabs is mandatory and it could be done resorting to π^- elastic scattering events. We expect to have $\geq$ 10 kHz of π^- scattered by the target and detected by the scintillator barrel. This prompt reaction is suitable for such a purpose. We then plan to use a prescaled trigger generated by the coincidence between the incoming π^- signal provided by the beam hodoscope and the one from the barrel when only one slab is fired (multiplicity 1) to collect the required high statistics data sample. Eventually the scintillator barrel could be equipped with a laser driven system for calibration purposes [46];

- in order to achieve a final time resolution better than 100 ps (rms), it is mandatory to determine and to continuously monitor the resolution function of the ToF detector. Events due to ^{3,4}He(π^-,$\pi^+\pi^-$)X reactions on the nuclear targets are produced with a factor $> 10^3$ with respect to the ^{3,4}He(π^-,$\pi^+\pi^-\pi^-$)$^{3,4}_{\Lambda}$H production and decay chain. A phase space simulation of the first process, with a total cross section of $\approx$ 20 mb at 1.05 GeV/c provided the above mentioned factor. These events should be tagged by a hit multiplicity 1 on the barrel, instead of 2 as for the reaction/decay process. The prompt ^{3,4}He(π^-,$\pi^+\pi^-$)X reactions can be exploited to determine the time resolution function, which will be used in the off-line analysis;

- the amplifier signals should also be sent to analog-to-digital converters (ADC) to permit the identification of the particles stopping in the range hodoscope modules, as explained in Section 9.

5.4 The range scintillator detector

The range detector system will be composed by four independent modules surrounding the liquid ^{3,4}He target and oriented parallel to the beam axis. Moving out from the beam axis, each module will be preceded by two high resolution drift chambers ($\approx 250\ \mu m$ (FWHM) resolution, x-y readout) spaced by 2-3 cm, to determine the incidence direction of the charged particles with a resolution of less than 100 mrad (FWHM): this will make possible to determine the momentum of the particles within 1.5-3%, as it will be shown in Section 7.

Each module will consist of thin scintillator planes of 40 cm $\times$ 60 cm cross section (perpendicular $\times$ parallel to the beam axis), with aluminized

mylar coating and spaced by air. The total scintillator thickness will be $\approx$ 10 cm to bring at rest π^- of 140 MeV/c maximum momentum and p up to 450 MeV/c momentum, which are the particles species and momentum ranges of interest to detect the K^0_S asymmetric decay, the ${}^{3}_{\Lambda}\mathrm{H}/{}^{4}_{\Lambda}\mathrm{H}$ two-body (three-body) MWD and the ${}^{4}_{\Lambda}\mathrm{H}$ NMWD.

The optimal geometry includes elements given by 3 mm thick scintillators spaced by air, giving a total module thickness $\leq$ 20 cm: this configuration should allow ease in positioning and handling the detector components while ensuring satisfactory performance in momentum resolution and particle identification accuracy. The total number of elements for each module would then be 34. An additional 3-5 mm thick scintillator will be placed as last element and its signal, put in anticoincidence, will be used as a veto for the particles which do not stop inside the range counter. Each plane will be divided in 5 cm width slices, alternately parallel and perpendicular to the beam, to obtain also information on the position of the hits for pattern recognition purposes.

The solid angle coverage will be $\sim (1.8 - 2)\pi$ sr.

5.5 The trigger strategy

The trigger strategy for the ${}^{3}_{\Lambda}\mathrm{H}/{}^{4}_{\Lambda}\mathrm{H}$ lifetime measurement is based on the following signals:

1. the logic OR of the discriminated signals of the tiles of the two beam hodoscope layers;

2. a signal elaborated from the ToF system slab MT's to determine the number of hit slabs (multiplicity);

3. a logic OR of the discriminated signals of the first layers (one or two layers in coincidence) of the range modules to indicate the presence of charged particles in the detector;

4. a veto signal from the additional layer at the end of each range module to identify particles which cross it without stopping;

5. a signal of the SKS downstream complex of detectors in a suited time window to identify π^+'s from the K^0_S decay.

These signals will feed different logic combinations to select events for the following purposes:

- to continuously monitor the time alignment of the ToF system slabs a prescaled trigger will be used, given by 1 .AND. 2 (mult=1) with a hit multiplicity of 1;

- to determine and to continuously monitor the response function of the ToF system for achieving a resolution better than 100 ps (rms): 1 .AND. 2 (mult=1) .AND. 5;

- to select events due to the production and decay of ${}^{3}_{\Lambda}$H/${}^{4}_{\Lambda}$H: 1 .AND. 2 (mult=2) .AND. 3 .AND. $\overline{4}$ .AND. 5.

6 Monte Carlo simulations

As mentioned in Section 5, a GEANT4 based simulation code was written in order to realistically model the geometry of the apparatus to be installed upstream the SKS complex. After that, the software program was used to simulate the physics process of interest and it is now being used to study the response of the different sub-detectors.

The implementation of an event generator able to reproduce the full chain of reactions (15), from the Λ-hypernucleus formation to its decay, is only apparently a trivial task. First of all, the process (15), where a Λ-hypernucleus is created inside the liquid ^{3,4}He target, was added to the list of the interactions that can be induced by the incoming π^- beam. Since the cross section for process (15) in the case of ${}^{3}_{\Lambda}$H is unknown, an artificial but reasonable interaction rate was assumed.

Then one had to face the problem that hypernuclei are not part of the GEANT4 standard set of particles and nuclei. The solution was to develop a customized version of the GEANT4 toolkit by adding ${}^{3}_{\Lambda}$H and ${}^{4}_{\Lambda}$H. For each of these two new objects, all the relevant physical properties and the main decay channels, properly normalized, were taken into account. Moreover, few core classes of the GEANT4 C++ library were modified in order to get ${}^{3}_{\Lambda}$H and ${}^{4}_{\Lambda}$H correctly transported across the volumes describing the experimental apparatus. Finally, particular care was put in checking that Λ-hypernuclei undergo to the right physical processes along their trajectories. As for as the stopping process of ${}^{3}_{\Lambda}$H and ${}^{4}_{\Lambda}$H in material is concerned, preliminary results were validated by comparing them with the output of the SRIM simulation code [43].

7 Expected apparatus performance

To measure the ${}^{3}_{\Lambda}$H/${}^{4}_{\Lambda}$H lifetime with the desired resolution, the apparatus should have good capabilities not only in measuring with high precision the delay time, but also in identifying the decaying system.

As already discussed, the formation of ${}^{3}_{\Lambda}\mathrm{H}/{}^{4}_{\Lambda}\mathrm{H}$ will be recognized by the missing mass of the production reaction (15):

$$m_{hyp} = [(E_{\pi^-} + m_A - E_{K^0_S})^2 - p^2_{hyp}]^{1/2} \tag{16}$$

where m_{hyp} stands for ${}^{3}_{\Lambda}\mathrm{H}/{}^{4}_{\Lambda}\mathrm{H}$ mass, m_A for the ^{3}He/^{4}He mass, E_{π^-} and $E_{K^0_S}$ for the total energy of the incoming π^- and of the outcoming K^0_S and p_{hyp} is the recoil momentum of ${}^{3}_{\Lambda}\mathrm{H}/{}^{4}_{\Lambda}\mathrm{H}$:

$$p_{hyp} = [p^2_{\pi^-} + p^2_{K^0_S} - 2p_{\pi^-}p_{K^0_S}\cos\theta_{\pi^- K^0_S}]^{1/2}. \tag{17}$$

Only events with a missing mass value falling in a suited interval centered on the known ${}^{3}_{\Lambda}\mathrm{H}/{}^{4}_{\Lambda}\mathrm{H}$ mass will be used for determining the lifetime. The width of this interval will depend upon the performance of the apparatus. In the same missing mass interval a background contribution will also be present, mainly due to the quasi free production of Λ on a proton of the target nucleus. The discussion of the background will be done in Section 12.

The momentum, and thus the energy, of the K^0_S will be evaluated by identifying it by means of the invariant mass of its decay (π^+, π^-) pair:

$$M_{K^0_S} = [m^2_{\pi^+} + m^2_{\pi^-} + 2(E_{\pi^+}E_{\pi^-} \; - \; p_{\pi^+}\; p_{\pi^-}\cos\theta_{\pi^+\pi^-})]^{1/2}. \tag{18}$$

The π^+ will be detected by the SKS in the forward direction corresponding to the spectrometer angular acceptance, (2°-14°) with respect to the beam axis, while the π^- will be detected by one of the range detector modules, at angles of about (60°-120°) with respect to the beam axis. The angle between the two tracks will be determined by measuring the outgoing π^+ and π^- directions by means of couples of drift chambers (a $\approx 250\ \mu m$ (FWHM) resolution can be expected) located in front of the SKS and of the hit range counter module. By assuming a resolution on the π^+ momentum of 0.2% (FWHM) for π^+ in the (650-690) MeV/c momentum range as quoted in [44], a resolution on the π^- momentum of about 3.5 MeV/c (FWHM) and a resolution on the angle of about 50 mrad (FWHM), the K^0_S invariant mass could be obtained with a resolution of 5-7 MeV (FWHM) ((1-1.5)%) depending on the angle between the two pions.

Moreover, the K^0_S momentum obtained by the sum of the measured pions momenta:

$$p_{K^0_S} = [p^2_{\pi^+} + p^2_{\pi^-} + 2p_{\pi^+}p_{\pi^-}\cos\theta_{\pi^+\pi^-}]^{1/2} \tag{19}$$

could be determined with a resolution of about 4-5 MeV/c (FWHM) ($< 1\%$). By considering a resolution on the π^- beam momentum of 0.2% (FWHM), a resolution on the ${}^{3}_{\Lambda}\mathrm{H}/{}^{4}_{\Lambda}\mathrm{H}$ missing mass of about 3.5-4.0 MeV (FWHM) should be obtained for K^0_S nearly collinear to the beam π^-. This resolution should

allow a good discrimination of the hypernucleus signal from the background, as discussed in Section 13.

The hypernucleus lifetime will be determined following the procedure sketched in Fig. 9. The time difference between the ${}^{3}_{\Lambda}\mathrm{H}/{}^{4}_{\Lambda}\mathrm{H}$ π^- from MWD

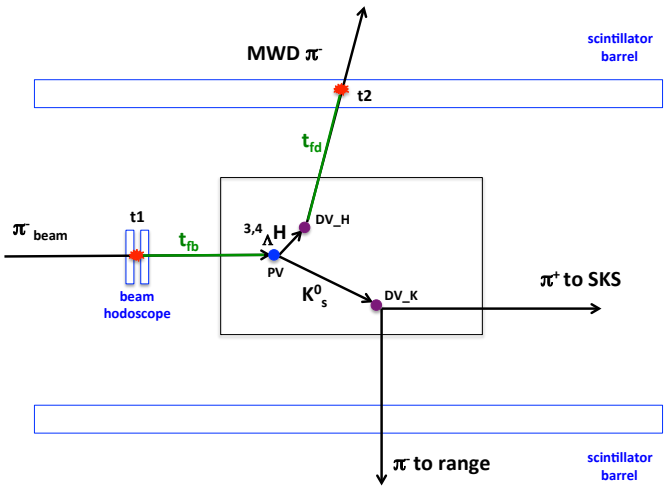

Figure 9: Scheme of the ${}^{3}_{\Lambda}\mathrm{H}/{}^{4}_{\Lambda}\mathrm{H}$ lifetime evaluation.

hitting the scintillator barrel, t_2, and beam π^- hitting the beam timing hodoscope, t_1, will be measured. The two scintillator hodoscope elements should have been previously aligned in time, within 50-60 ps (rms) each, and the resolution on the time difference should be ∼70-90 ps (rms). Its knowledge as well as the monitoring of its stability is of paramount importance: prompt reactions will be used for both purposes as it will be explained in more details in Section 10.

The time difference will be then corrected, event by event, to take into account the beam flight time between the timing hodoscope and the production vertex PV, t_{fb}, and the weak decay π^- flight time between the hypernucleus decay vertex DV_H and the scintillator barrel slab, t_{fd}. By the way, it is worth to mention that, according to the GEANT4 simulation, the mean flight path of the ${}^{3}_{\Lambda}\mathrm{H}$ in liquid ${}^{3}\mathrm{He}$ target amounts to ≈ 8 mm, while is ≈ 4 mm for ${}^{4}_{\Lambda}\mathrm{H}$ in liquid ${}^{4}\mathrm{He}$. The hypernucleus lifetime will be evaluated from the distribution of the corrected time difference:

$$t({}^{3}_{\Lambda}\mathrm{H}/{}^{4}_{\Lambda}\mathrm{H}) = (t_2 - t_1) - t_{fb} - t_{fd}. \qquad (20)$$

To determine t_{fb} first of all the K^0_S decay vertex, DV_K, will be obtained by the intersections of its decay π^+ and π^- momentum vectors, already considered for the K^0_s invariant mass calculation. Moving back from the K^0_S decay vertex, the known K^0_S momentum will intersect the known beam direction in a point which corresponds to the hypernucleus production vertex PV; the flight time t_{fb} will be evaluated from the distance between the position of the hit on the beam hodoscope and PV, by considering the known beam momentum. (a second order correction will be given by considering the almost negligible beam particles slowing down in the LHe).

To determine t_{fd} the K^0_s momentum vector will be considered once more. From simple two-body reaction kinematics considerations, the hypernucleus momentum vector will be calculated as the difference between beam and K^0_S momentum vectors, thus evaluating the ${}^3_\Lambda$H/${}^4_\Lambda$H emission direction. The intersection of this emission direction and the weak decay π^- momentum vector direction will allow to determine the DV_H position; the decay π^- flight length will be determined from DV_H and the position of the hit on the scintillator barrel slab. The flight time will be calculated from this flight length and the decay π^- momentum measured by the range array.

Thanks to the localizing capability of the drift chambers, the uncertainty introduced by the corrections can be evaluated in first approximation by considering that each flight length is determined with an error of $\approx$ 1 mm (rms) which corresponds to an uncertainty on t_{fb} of $\approx$ 3 ps (rms) and on t_{fd} of $\approx$ 5-8 ps (rms) for decay π^- in the (70-140) MeV/c momentum range. The global uncertainty due to corrections would be $\approx$ 6-8 ps (rms) and it would give an overall resolution on the delay time of $\lesssim$ 100 ps (rms) and an error on the hypernucleus lifetime of $\approx$ 3-4% with 1000 entries.

8 ${}^3_\Lambda$H and ${}^4_\Lambda$H yields

The main difficulty in planning the measurement is the correct evaluation of the expected ${}^3_\Lambda$H yield. Indeed, the cross section for the process (15) is actually unknown in the case of ${}^3_\Lambda$H production. In order to get a realistic estimate of its value, one can remind that a prediction based on a DWIA calculation was done for the cross section of the ^{4}He$(\pi^+,K^+){}^4_\Lambda$He reaction [47], which is the isospin symmetric of the ^{4}He$(\pi^-,K^0){}^4_\Lambda$H process. It reaches the quite large value of $\approx$ 10 μb/sr for incident π^- momentum ranging between 1.0 and 1.1 GeV/c and when K^0_S is emitted at 4° with respect to the beam direction. Then, a plausible value for the differential cross section of reaction (15) is 10 μb/sr for ${}^4_\Lambda$H and a reasonable guess for ${}^3_\Lambda$H could be $\approx$ 5 μb/sr.

The number of ${}^3_\Lambda$H and ${}^4_\Lambda$H which can be produced in the described ap-

paratus acceptance is given by:

$$\begin{aligned} \text{yield}({}^{3}_{\Lambda}\text{H}/{}^{4}_{\Lambda}\text{H}) &= N_{\pi^-} \times \frac{T_{\text{tar}}}{A} \times N_A \times \frac{d\sigma}{d\Omega} \times \Omega_{\text{spe}} \times \varepsilon_{\text{spe}} \times \varepsilon_{\text{rec}} \\ &\approx 2.6 \times 10^3 \quad \text{and, respectively,} \quad \approx 2.0 \times 10^3 \end{aligned}$$

where

- $N_{\pi^-} \equiv$ number of π^- delivered on target $\approx 5.2 \times 10^{12}$ and $\approx 1.7 \times 10^{12}$
- $T_{\text{tar}} \equiv$ liquid ^{3}He/^{4}He target thickness = 0.81 g/cm^2 and 1.25 g/cm^2,
- $A \equiv$ ^{3}He/^{4}He atomic weight,
- $N_A \equiv$ Avogadro constant,
- $\frac{d\sigma}{d\Omega} = 5$ μb/sr and 10 μb/sr,
- $\Omega_{\text{spe}} \equiv$ spectrometer solid angle coverage (SKS) ≈ 0.1 sr,
- $\varepsilon_{\text{spe}} \equiv \text{BR}(K^0 \to K^0_S) \times \text{BR}(K^0_S \to \pi^-\pi^+) \times (\pi^-\pi^+)$ pair detection probability ≈ 0.01
- $\varepsilon_{\text{rec}} \equiv$ reconstruction algorithm efficiency ≈ 0.7.

By taking into account the available branching ratios values for the ${}^{3}_{\Lambda}$H and ${}^{4}_{\Lambda}$H MWD channels, (1) and (3) and, respectively, (7) and (9), it is possible to estimate the number of useful events for the $\tau({}^{3}_{\Lambda}\text{H})$ and $\tau({}^{4}_{\Lambda}\text{H})$ measurement. The decay products from two- and three-body processes will be detected by the range counter only, then the number of observed ${}^{3}_{\Lambda}$H and ${}^{4}_{\Lambda}$H decays is given by:

$$\begin{aligned} \text{yield(decaying } {}^{3,4}_{\Lambda}\text{H)} &= \text{yield}({}^{3,4}_{\Lambda}\text{H}) \times \text{BR}({}^{3,4}_{\Lambda}\text{H} \to \text{2-/3-b}) \times \frac{\Omega_{\pi^-}}{4\pi} \times \varepsilon_{\pi^-} \times \varepsilon_{\text{rec}} \\ &\approx 6.0 \times 10^2 \quad \text{and, respectively,} \quad \approx 5.0 \times 10^2, \end{aligned}$$

where

- $\text{BR}({}^{3}_{\Lambda}\text{H} \to \text{2-/3-b}) \equiv$ two- and three-body decay branching ratio ≈ 0.25 [2] and, respectively, ≈ 0.40 [2],
- $\text{BR}({}^{4}_{\Lambda}\text{H} \to \text{2-/3-b}) \equiv$ two- and three-body decay branching ratio ≈ 0.49 [48] and, respectively, ≈ 0.22 [48],

- $\frac{\Omega_{\pi^-}}{4\pi} \equiv$ range detector solid angle coverage for $\pi^- \approx 0.5$,

- $\varepsilon_{\pi^-} \equiv \pi^-$ detection efficiency ≈ 1,

- $\varepsilon_{\rm rec} \equiv$ reconstruction algorithm efficiency ≈ 0.8.

Then, by adding the two- and the three-body decay events we expect to have $\approx 5.0 \times 10^2$ entries in the correspondent time delay spectra for both ${}^{3}_{\Lambda}$H and ${}^{4}_{\Lambda}$H. Such a number of collected events is the minimum data sample necessary to determine $\tau({}^{3}_{\Lambda}{\rm H})$ and $\tau({}^{4}_{\Lambda}{\rm H})$ with a statistical error of few percent, as summarized in Table 3. With the beam intensity that we can handle, namely 1.0 $\times 10^7$ π^- / spill and a 5 s accelerator cycle operation, the request translates in a beam time allocation of 30 days and of 10 days for the ${}^{3}_{\Lambda}$H and the ${}^{4}_{\Lambda}$H study respectively.

Table 3: Minimum expected Λ-hypernuclei production rates for a given number of data taking days and for different targets. The numbers listed in column 5 indicate the statistical significance of the measurement that can be achieved for $\tau({}^{A}_{\Lambda}Z)$ with the present beam intensity (1.0 $\times 10^7$ π^- per spill and 5 s accelerator cycle operation).

beam request (days)	target	thickness (g/cm^2)	detected ${}^{A}_{\Lambda}Z$ decays	statistical significance (%) $\tau({}^{A}_{\Lambda}Z)$
30	L ^{3}He	0.81	$\lesssim 6 \times 10^2$ ${}^{3}_{\Lambda}$H	$\gtrsim 4.0$
10	L ^{4}He	1.25	$\lesssim 5 \times 10^2$ ${}^{4}_{\Lambda}$H	$\gtrsim 4.5$

9 Momentum measurement and particle identification in the range detector

The range scintillator array will permit to identify and to measure the momentum of the particles which slow down and stop inside its material. From a logical point of view, the particle identification has to be performed as a starting point of the momentum reconstruction procedure which consists of three steps: to identify the particle type (pion/proton), to measure the incidence angle of the identified particle, to use the range table of the identified particle impinging with a known angle to determine its momentum, as a function of the number of crossed layers.

The range detector particle identification capabilities have been optimized to distinguish pions coming from the K^0_S decay and from the ${}^{3}_{\Lambda}$H/${}^{4}_{\Lambda}$H MWD

from the protons coming from the NMWD. For pions, momenta in the (70-140) MeV/c range have been considered; for protons in the (250-500) MeV/c range. The particle identification algorithm is built by correlating the en-

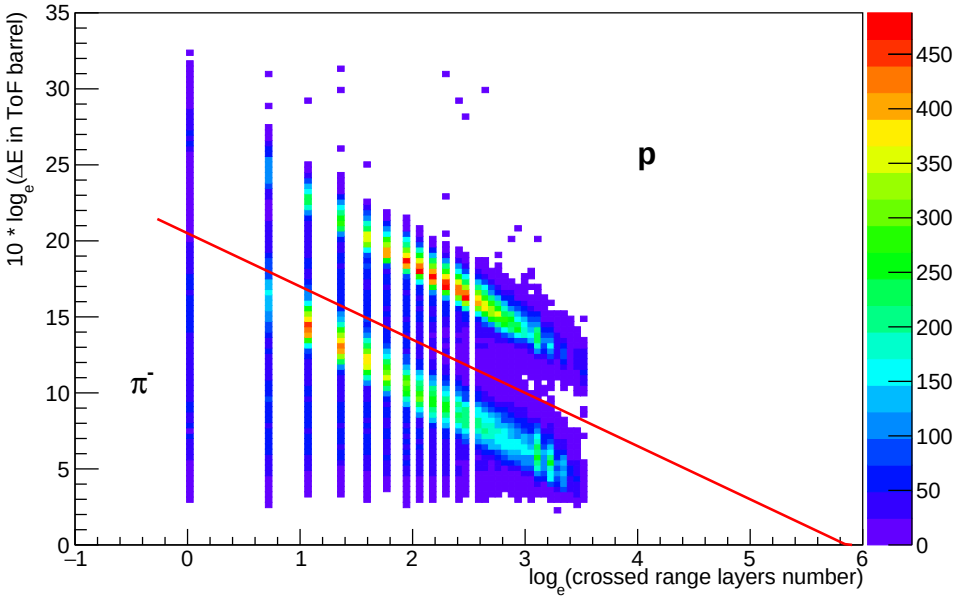

Figure 10: PID algorithm: $(log_e(number\ of\ crossed\ range\ layers), 10 \times log_e(\Delta E_{ToF}))$ for 3 mm thick range scintillator layers.

ergy loss in the 5 mm thick staves of the scintillator barrel used for the time of flight measurement and the number of crossed 3 mm thick layers in the range array. Fig. 10 shows the two dimensional plot of $10 \times log_e(\Delta E_{ToF})$ versus $log_e(nlayers)$, taken into account for events, simulated with the Geant4 toolkit [42], in which a couple (π^-, p) generated in the liquid He target is hitting the range modules. As it can be clearly seen, pions and protons populate two different regions, well separated by a straight line whose equation will be determined at the calibration stage and will be used for the identification. When applying it to simulated data, efficiencies of $\epsilon_\pi \approx 99.6\%$ and $\epsilon_p \approx 97.6\%$ are obtained for pions and protons; contamination levels of about 2.4% is found for pions, corresponding to misidentified protons and of less then 1% for protons due to misidentified pions. Finally a purity of about 97.5% is found for pions and of about 99.5% for protons.

Once the particle is identified, its momentum will be calculated based on the range table for its species. The table contains the number of crossed

layers for pions or protons of known momentum, impinging on the range with a known angle. Also in this case, a dedicated simulation allowed to build the tables for pions and protons in the above mentioned momentum ranges. The granularity for the momentum has been chosen as 5 MeV/c for pions and 15 MeV/c for protons, while a 5 degrees step has been used for the incidence angles in both cases. A linear interpolation algorithm is applied for intermediate crossed layers numbers to improve the performance. During the data reconstruction process the incidence angle will be obtained

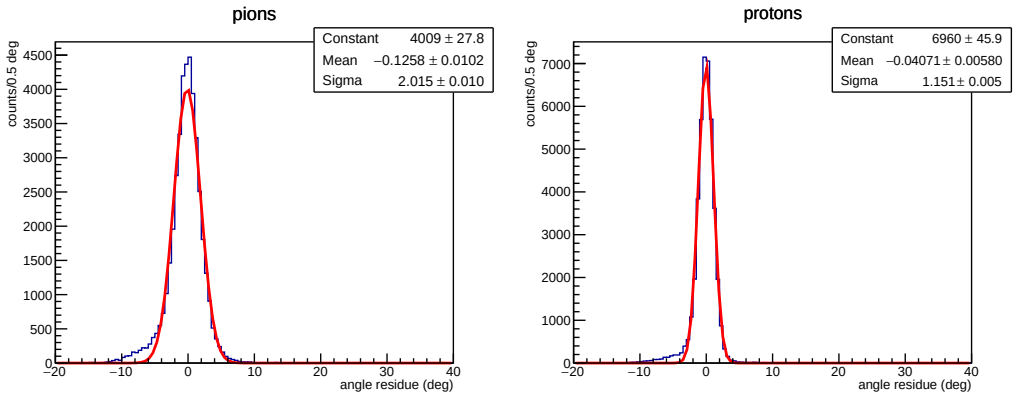

Figure 11: Residue of the incidence angle of isotropically generated pions/protons on the range modules: the simulated angle is subtracted from the reconstructed one. On the left the residue for pions, on the right for protons.

from the points of the high resolution drift chambers pairs located in front of each range module. Fig. 11 shows the residue between the reconstructed and the simulated incidence angle, obtained by assuming a drift chamber space resolution ≈ 250 μm (FWHM) when the full assembly of four range modules is considered and particles are generated isotropically inside a region corresponding to the liquid ^{4}He target. For pions a gaussian residue distribution is obtained with a mean smaller than 1 degree, which can be considered as a systematic error in the angle reconstruction, and a standard deviation of about 2 degrees. Also for protons a mean smaller than 1 degree is obtained, while the standard deviation reduces to about 1 degree. Finally, Fig. 12 shows the reconstructed momentum residue obtained for pions and protons. In the upper panel, the correlation existing between the momentum residue and the simulated momentum is shown. In the lower left panel the residue distribution for pions is shown, with a mean value of about 2 MeV/c, which can be considered as a systematic error due to the momentum reconstruction

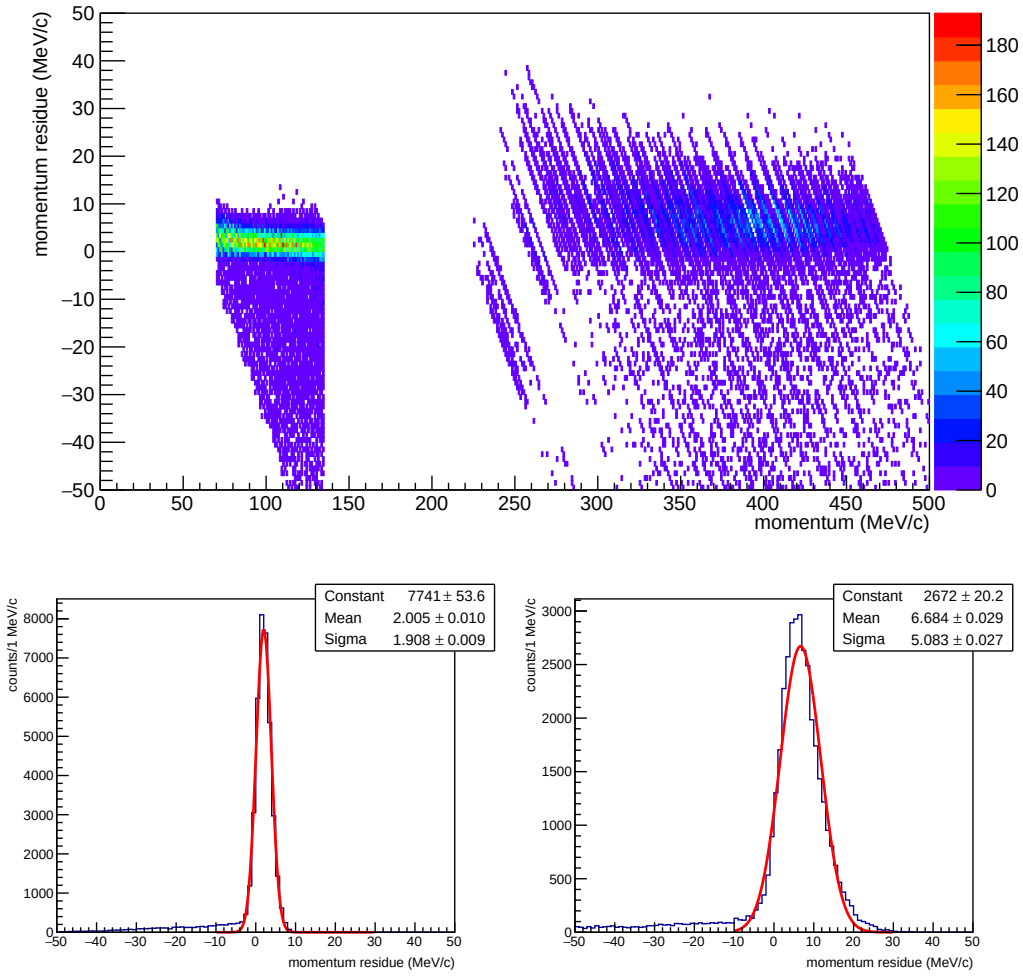

Figure 12: Residue of the momentum reconstructed by the range detector for pions and protons generated in the (70-140) MeV/c and (250-500) MeV/c range respectively. See the text for more details.

algorithm, and a standard deviation of about 1.9 MeV/c which corresponds to 1.4-2.8% of the simulated momentum range. In the lower right panel the residue distribution for protons is shown, with a mean value of about 6.7 MeV/c and a standard deviation of about 5.0 MeV/c, corresponding to the same relative uncertainty.

10 Calibration of the apparatus

The experimental apparatus will need calibration tools for the following subsystems:

- time alignment of the beam hodoscope elements to better than 80 ps;
- time alignment of the scintillator hodoscope barrel staves to better than 80 ps;
- response function of the ToF system to achieve its intrinsic resolution (prompt reactions, pion inelastic scattering);
- response function of the range array for pions and protons of known incidence angle and momentum (test beam and simulations).

The first two items will contribute to the time response function width of the ToF system. The first item is related to the small beam hodoscope elements and it will likely be addressed through electronic techniques. The second and third items will be addressed by resorting to π^- elastic scattering and to ^{3,4}He(π^-,$\pi^+\pi^-$)X events, as described in Subsection 5.3. It is worth to remind that in order to determine the intrinsic resolution of the ToF system response function the corrected delay times of the prompt reactions should be used, following the simplified procedure outlined in Section 13.

To approach the fourth item it is important to notice that the very good performance of the momentum reconstruction is supported by the thin granularity of both angle and momentum samplings of the range tables, which allows to apply a reliable linear interpolation. A coarse granularity can be used, but steps smaller than 10 degrees for the angle and 10 MeV/c and 25 MeV/c for pions and protons momentum must be used to obtain a reconstructed momentum resolution less than 5%.

To our knowledge it is not possible to perform calibration runs in realistic conditions since no pion beams are available in the (70-140) MeV/c momentum range. Then the strategy should be to perform a fine tuning calibration, with the needed granularity, for the proton table at existing proton machines like RCNP, J-PARC or LNL test beam facilities: indeed, it should not be difficult to measure some elements of the simulated table to verify if it is in good agreement with direct determinations. Since the simulation from which both pion and proton tables have been obtained only describes the well known ionization energy loss process, no particular issues are expected. Also the reliability of the PID algorithm (see Fig. 10) could be directly tested for protons of some known momentum values. When the reliability of the simulated behavior of protons in the range array will be assessed. In

addition, due to the simplicity of the simulation, also the pion table could be accepted.

11 Analysis of the data

The analysis of the data will be structured in three main steps, intended to identify events in which an incoming π^- interacts with a ^{3,4}He nucleus to produce a ${}^{3}_{\Lambda}\mathrm{H}/{}^{4}_{\Lambda}\mathrm{H}$ hypernucleus and a K^0_S which decays in a $\pi^+\pi^-$ pair with an asymmetric topology; then, the decay of the hypernucleus is considered.

The starting point will be to search for events with three charged particles in the final state: a π^+ entering the SKS spectrometer (angular and momentum acceptance) which measures its momentum, a first π^- detected in the range array, emitted at (60°-120°) with respect to the π^+ in the K^0_S decay and a second π^- detected in the range array and coming from the two- and from the three-body ${}^{3}_{\Lambda}\mathrm{H}/{}^{4}_{\Lambda}\mathrm{H}$ MWD, or a proton coming from the NMWD channels.

When the MWD is considered, in order to identify the π^- coming from the K^0_S decay, the invariant mass of the π^+ and each π^- will be calculated; this way, the one giving a value closest to the K^0_S mass [3] will be regarded as the π^- from the K^0_S decay. Since the two π^-'s have very similar momenta, in particular in the case of the two-body MWD of the hypernucleus, a high resolution is needed in the invariant mass calculation: this justifies the use of two high resolution drift chambers pairs to determine the pions momentum directions and then the angle between the two vectors. Also the K^0_S momentum vector will be determined by summing the two decay pions momenta.

Once the K^0_S has been reconstructed, the ${}^{3}_{\Lambda}\mathrm{H}/{}^{4}_{\Lambda}\mathrm{H}$ missing mass will be calculated by using the beam π^- vector momentum. Also in this case, a good resolution on the missing mass will allow to reduce the contamination due to background reactions, mainly the Λ quasi-free production and decay which mimic quite closely the hypernuclear events.

For the events whose missing mass will fall in a fiducial interval centered on the known hypernucleus mass, the arrival time on the scintillator barrel of the π^- not associated with the K^0_S decay, or of the proton from NMWD, will be considered to fill the delay time spectrum:

$$t_2 - t_1 = t_{fb} + t({}^{3}_{\Lambda}\mathrm{H}/{}^{4}_{\Lambda}\mathrm{H}) + t_{fd} \tag{21}$$

where the same notation of Section 7 is used, namely: t_2 is the arrival time of the hypernucleus decay π^-/p onto the ToF scintillator barrel, t_1 is the time given by the beam π^- crossing the beam hodoscopes, t_{fb} is the flight time

of the beam π^- from the beam hodoscope to the reaction vertex, $t(^3_\Lambda\mathrm{H}/^4_\Lambda\mathrm{H})$ is the hypernucleus life time (flight time from the production vertex to the decay vertex) and t_{fd} is the flight time of the decay π^-/p from the decay vertex to the ToF hodoscope. If the hypernucleus will decay through the NMWD, there will be no ambiguity between the two decay particles in the range array. In this case, the NMWD branching ratio could be evaluated by exploiting the detected MWD π^- number and the known MWD branching ratio to count the produced hypernuclei.

12 Expected backgrounds and their control

The level of expected background from the $^{3,4}\mathrm{He}(\pi^-,\pi^+\pi^-)\mathrm{X}$ reactions has been discussed in Subsection 5.3. The frequency of such processes has been estimated to be a factor 10^3 larger than the $^{3,4}\mathrm{He}(\pi^-,\pi^+\pi^-)^{3,4}_\Lambda\mathrm{H}$ production and decay chain (15). Since the main selection criterion of the final trigger is the multiplicity of the fired scintillator slabs (2 for the event of physics interest, 1 for the others), it is possible to think that the number of the spurious triggers can be reduced by at least one order of magnitude by choosing a suitable level of segmentation of the ToF barrel. This way, the data acquisition system will have to manage reasonable numbers. Finally, the unwanted events will be rejected during the off-analysis procedure, which as usual will take into account all the physical and kinematical constraints. Other reactions, producing more than 3 pions in the final state, or other even more exotic configuration have very small yields for phase space considerations or, respectively, the need of a coherent production on the nuclei, with vanishing cross section.

A further source of background is represented by the flux of particles irradiating the various arrays of detectors. In the following, we only outline some straightforward requirements, aiming to reduce its impact. The main coincidence driving the timing and the gating of all the subsystems will be given by a π^- detected by the incident beam counters with a π^+ signal from the array of detectors at the exit of the SKS complex. In order to account for the different length of trajectories and for the different momenta of the π^+ falling in the spectrometer acceptance, the time width of the coincidence must be of the order of 10 ns. Following the existing literature [49], we assume that about 2% of the beam would interact in the target [50], with a roughly 90% probability of emission in a forward cone not subtended by the range scintillator hodoscope arrays. The interacting beam fraction would produce a coincidence rate, between the incident π^- beam and an outgoing π^+ accepted by the SKS, $\approx 10^{-5}$ times the incident flux. Each of the four

range modules will be irradiated by a total number of 5×10^{-4} times the flux of beam particles. Depending on the capabilities of the DAQ system, this minimum bias trigger could be used to collect data, leaving background events to be rejected by subsequent on- and off-line analyses.

Furthermore, a reduction of more than 2 orders of magnitude could be reached by adding the request of an anticoincidence between the first one or two layers and the last thicker one of each range module. This requirement excludes all charged particles not stopping in the hodoscope. The rate expected from the use of such a trigger will be $\approx 10^{-7}$ times the flux of beam particle. It would be compatible with the number of random coincidences. Indeed, the range scintillator hodoscope ensemble will be irradiated by 2×10^{-3} times the flux of beam particles. The rate of random coincidences entering the trigger will be of 4×10^{-16} times the (flux of beam particles)^2. This number is fully acceptable, even though it is a lower limit due to the beam time microstructure during the spill duration. However, these numbers are large when compared with the true events expected for the production and decay of ${}^{3}_{\Lambda}$H and ${}^{4}_{\Lambda}$H, discussed in the previous Section 8. The background will be strongly reduced in the off-line analysis which will take into account the ADC and TDC spectra and their correlations for all the elements of the range scintillator hodoscope. A quantitative determination of the performance of such off-line selection will be done following the completion of the full simulation of the detector layout and response, currently in progress. We mention that the impact of background events on the systematic error in the final value of the lifetime will be determined in the final analysis of the time delay spectra discussed in Section 13.

A second source of background, that we may define as topological, is related to the fact that the range scintillator hodoscope is used to detect both the π^- from the K^0_S decay (π^-_1) and from the ${}^{3}_{\Lambda}$H or ${}^{4}_{\Lambda}$H MWD (π^-_2), emitted in a similar momentum range. Possible ambiguities that could force rejection of these events may occur. Since the two π^- are uncorrelated, the probability that both are detected by the same module is $\approx 25\%$ for the 4 modules. Furthermore, the direction of π^-_1 is closely related to the direction of the π^+ detected by SKS, while that of π^-_2 is not. Thus we expect that at least a factor 20 reduction will be achieved by requiring the angular correlation corresponding to the $K^0_S \to \pi^+\pi^-$ decay. This simple topological constraints should reduce the ambiguities to the level of 1%. If necessary, a further selection on the $\pi^+\pi^-_{1,2}$ invariant masses can be applied (see Section 11).

13 Analysis of the time spectra

We start the discussion on the analysis of the time spectra (20), from which the observable τ is determined, by taking as example the case of ${}^{4}_{\Lambda}$H for reasons of simplicity. The analysis strategy can follow two different approaches.

In the first one, we will search for the ${}^{4}_{\Lambda}$H two-body decay (7) (B.R. $\approx 49\%$) at rest. Even though, according to the GEANT4 simulation, the number of such events is $\lesssim 20\%$ of the decaying ${}^{4}_{\Lambda}$H, they provide a monokinetic π^- of 132.9 MeV/c. They can be effectively selected by looking for π^- comprised in a small interval, whose width corresponds to the resolution of the range array detector, and by accepting MM values falling within the range corresponding to the ${}^{4}_{\Lambda}$H mass. This way it will be possible to be sure, within 1-2%, that such events are due to ${}^{4}_{\Lambda}$H two-body decay. However, due to the finite resolution of 3.5-4.0 MeV (FWHM), events from the Λ free decays will be present. In order to estimate such a contamination, following the hypothesis of Ref. [51] for the isospin symmetric (π^+,K^+) reaction, we assume that the spectrum of π^- corresponding to the unbound region up to 15 MeV has the same shape and it amounts to 10 times the ${}^{4}_{\Lambda}$H peak content. About 1% of the Λ free decay events (typically 10^2 out of 10^3 populating the peak) will produce π^- which overlap the narrow distribution of the π^- following the ${}^{4}_{\Lambda}$H decay. The momentum of background π^- was found, according simulations, to have a rather flat distribution up to ≈ 170 MeV/c. Then, we expect that in the time delay spectra of the two-body decay there will be a contamination of the order of 2-3% due to Λ free decay, which is negligible. In this case, if we assume that the hypernucleus decay rate follow a probability distribution:

$$P(t) = \frac{1}{\tau} \exp^{-t/\tau}, \tag{22}$$

where τ is the mean life and $P(t)$ is the decay rate at a time t, the actual time delay distribution can be fitted to:

$$S(t) \;=\; \int_0^\infty A \, \frac{1}{\tau_{hyp}} \exp^{-t'/\tau_{hyp}} R(t-t') \; dt' \tag{23}$$

where $R(t-t')$ is the detector time response function and A is the normalization factor.

Fig. 13 shows a fit to a simulated distribution with $\tau({}^{4}_{\Lambda}\mathrm{H}) = 190$ ps, obtained with 5×10^2 events, by assuming that the detector time response function is a Gaussian with $\sigma = 100$ ps. This last hypothesis is supported by the results obtained in previous similar experiments [45, 65]. Statistical and systematic errors $\leq 1\%$ and, respectively, 7.8% have been inferred.

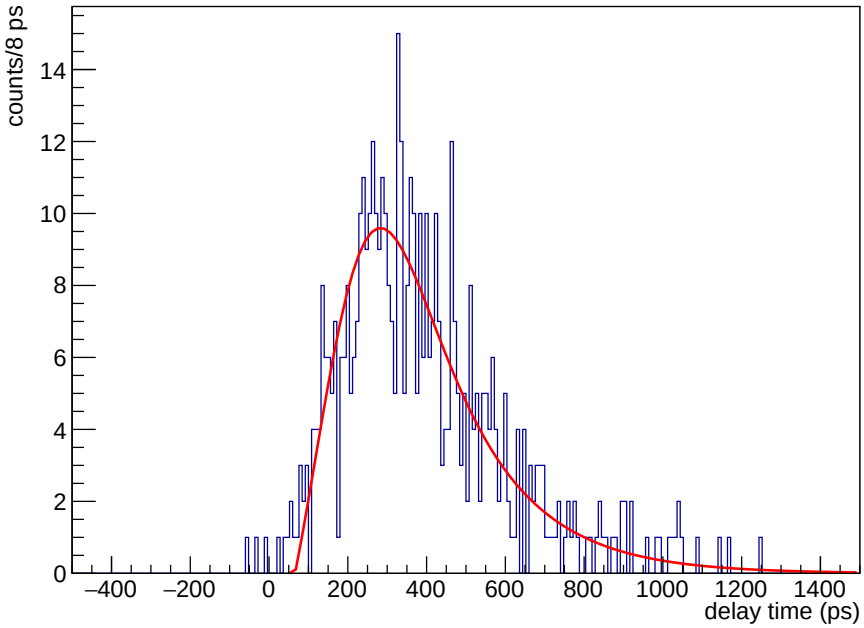

Figure 13: Outcome of the convolution fitting procedure of a time delay spectrum given by a gaussian response function with a resolution of ≈ 240 ps (FWHM) and a negative exponential distribution with a τ value of 190 ns and corresponding to 5×10^2 events.

In the second approach, in order to use all the collected events, the full spectrum of possible π^- decay channels, including in-flight two-body decay, will be studied. In this case the selection criteria on the π^- have to be relaxed and thus the contamination from Λ quasi-free decay will increase up to $\approx 20\%$ or even more. Then, a fit with two exponentials, one fixed at the $\tau(\Lambda_{\text{free}})$ value, should be done on the time delay spectra. If we assume that both the hypernucleus and the free Λ decay rate follow the same probability distribution (22), the time delay distribution can be fitted to:

$$S(t) \;=\; \int_0^\infty \left(A\,\frac{1}{\tau_{hyp}} \exp^{-t'/\tau_{hyp}} \;+\; B\,\frac{1}{\tau_\Lambda} \exp^{-t'/\tau_\Lambda} \right) R(t-t')\; dt' \quad (24)$$

where A and B give the weights of the two components. Finally, the hypernucleus lifetime $\tau_{hyp} = \tau({}^4_\Lambda\text{H})$ can be obtained from the fit.

A comparison of the values obtained in the two different approaches could in addition permit the evaluation of possible systematic errors in the deter-

mination of $\tau(^4_\Lambda\mathrm{H})$ with the continuous π^- decay spectra.

In order to check the reliability of the two-exponentials fitting procedure of the full decay π^- spectrum, the time delay spectrum obtained by displacing the cut on the selection on the MM spectra by some MeV should be analyzed. This way, it should include all backgrounds contributions and it would exclude $^4_\Lambda$H decays. By subtracting this time spectrum corresponding to the quasi-free region, properly normalized, from the previous one obtained for the $^4_\Lambda$H peak, it will be possible to fit the full time delay difference spectrum to a single exponential, which corresponds to $\tau(^4_\Lambda\mathrm{H})$. In this respect, a possible dependence of the Λ momentum on the MM value of the quasi-free process should be accounted for.

We expect a situation certainly worse for the $^3_\Lambda$H case, due to its very low B_Λ value. From the analysis of Ref. [51] and from the experimental data on the $(e,\ e'K^+)$ reaction on ^{3}He [37] we expect that in the selected MM peak there will be a nearly equal number of events due to $^3_\Lambda$H formation and to Λ free production. On the basis of the same aforementioned arguments, we may expect a 10% contamination in the time delay spectra of the $^3_\Lambda$H two-body decay events (p_{π^-} from (1) $\approx$ 114.4 MeV/c) and a 90% contamination level in the continuous π^- distribution corresponding to three- and four-body decay. In both cases a fit with two exponentials will be necessary, once the method has been validated by studying $^4_\Lambda$H. In the end also for $^3_\Lambda$H the global time delay spectrum could be considered with the advantage of recovering a consistent part of the three-body decay statistics, limited only by the low momentum acceptance cut of the range array detector.

We should use the same method of analyzing the time delay spectra obtained by displacing the cut on the selection on the MM spectra mentioned from $^4_\Lambda$H to asses the systematic error.

A Possible measurement of the lifetime for medium to heavy neutron-rich Λ hypernuclei

We briefly discuss here some measurements on other nuclear targets that would be feasible with the outlined apparatus. They should allow the determination of the lifetime and of the π^- and one-proton induced WD rates for several p-shell hypernuclei. These hypernuclei lie at the interface between the regions $\mathrm{A} \leq 5$ (s-shell), in which the Pauli principle does not act significantly and the MWD dominates, and $\mathrm{A} \geq 16$, in which the Pauli principle starts to inhibit significantly the MWD while NMWD dominates. Detailed

reviews may be found in Refs. [6–8]. For p-shell hypernuclei a strong theoretical effort was done more than 20 years ago. Accurate calculations were performed evaluating the observables which could be measured, in particular Γ_{π^-} and Γ_{π^0}. The main results, with a detailed list of all relevant references may be found in Ref. [52]. Those theoretical calculations were nicely confirmed only recently by measurements reported in Ref. [53] of Γ_{π^-} for several p-shell hypernuclei. Fig. 14 reports the experimental results, as taken by

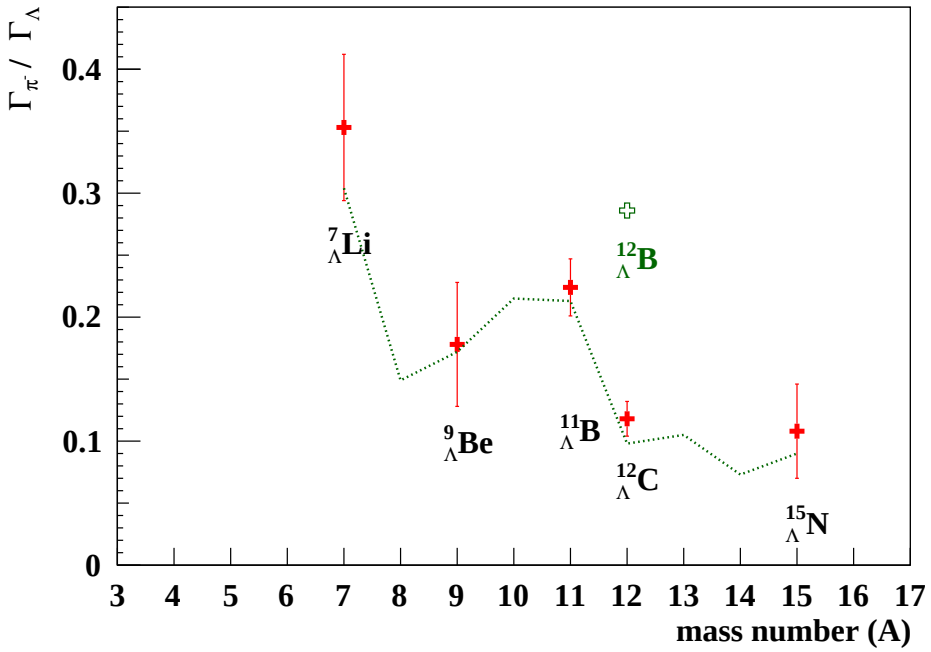

Figure 14: World average of the experimental $\Gamma_{\pi^-}/\Gamma_\Lambda$ values (red crosses) for different p-shell Λ-hypernuclei. The green dotted line and the open cross marker represent the theoretical prediction of $\Gamma_{\pi^-}/\Gamma_\Lambda$ [52] for the already studied Λ-hypernuclei and, respectively, for the still unmeasured ${}^{12}_{\Lambda}$B.

the survey of Ref. [8] compared to the theoretical predictions summarized in Ref. [52]. A substantially good agreement is found. Being characterized by a small Q-value, the MWD mode is strongly affected by the details of both the hypernucleus and the daughter nucleus structure. Theoretical calculations were based on the π-mesonic interaction introduced by Dalitz [54]. Pion final state interactions were taken into account by using pion waves distorted by the pion-nucleus optical potential. The structure of the nuclear core was described with the Cohen-Kurath spectroscopic approach [55]. For p-shell hypernuclei it was found that the total π^- decay rate is dominated by $\Lambda(1s) \rightarrow p(1p)$ transitions while only small contributions are given

by higher-energy configurations of the final nuclear system, mainly through $\Lambda(1s) \rightarrow p(2s, 1d)$ transitions. Strong nuclear shell structure effects, mainly due to the Pauli blocking of the various proton transitions, are already visible in the existing data on Γ_{π^-}. Charge dependence effects are also evident in the existing values of the ratio $\Gamma_{\pi^-}/\Gamma_{\pi^0}$. From Ref. [56] we obtain 1.19 ± 0.37 for ${}^{11}_{\Lambda}$B and 0.725 ± 0.091 for ${}^{12}_{\Lambda}$C, remarkably different from the value of 2 expected by the simplest approximation of the interaction (no shell effects and no distortion).

Strong effects were predicted for the mirror hyperisobars ${}^{12}_{\Lambda}$B and ${}^{12}_{\Lambda}$C due to the different decay schemes shown by Fig. 15. A recent precise evaluation

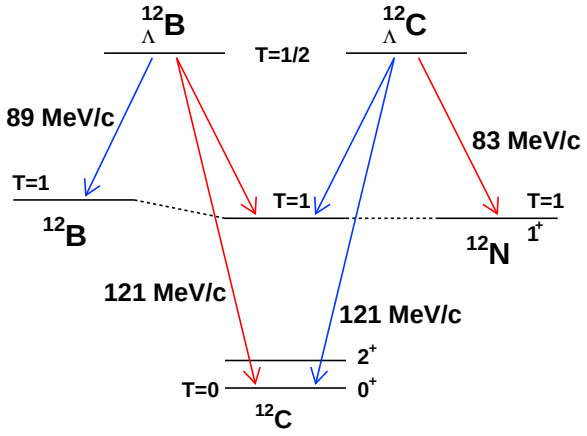

Figure 15: ${}^{12}_{\Lambda}$B and ${}^{12}_{\Lambda}$C MWD schemes: red arrows indicate charged MWD, black arrows neutral MWD.

of $\Gamma_{\pi^-}({}^{12}_{\Lambda}\mathrm{B})/\Gamma_{\pi^-}({}^{12}_{\Lambda}\mathrm{C})$ which took into account all the details of the interaction provided the value of 2.9 [52]. In addition, even though to a lesser extent due to the higher momentum transfer, nuclear structure effects are predicted for the one-nucleon induced NMWD widths and for τ too [52].

The experimental layout described for exploiting the reaction (π^-, K^0) is adequate to produce ${}^{12}_{\Lambda}$B and to measure precisely τ, Γ_{π^-}, Γ_p. Up to four targets of ^{12}C (graphite) could be arranged within the cylindrical volume used to host the liquid ^{3}He/^{4}He target, as sketched in Fig. 16. They should be about 4 mm thick each and tilted by 15-20 degrees with respect to the beam axis, as done in previous experiments with the (π^+, K^+) reaction [57], in a sort of "Venetian blind" arrangement. This way, the thickness seen by the beam particles will be maximized whereas that seen by the charged particles emitted in the decay will be minimized.

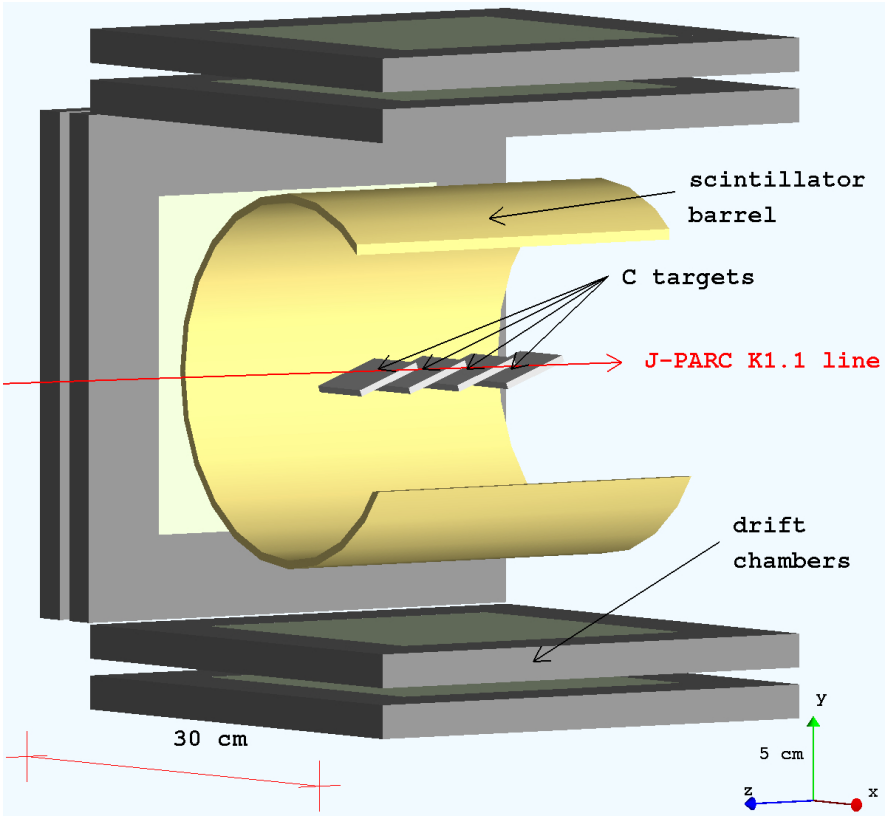

Figure 16: Magnified schematic view of the targets layout for the decay measurements on p-shell hypernuclei with the (π^-, K^0) reaction, as it is currently implemented in the GEANT4 simulation program. One of the quadrant of the apparatus has been removed to permit to see the interior details.

For the cases of a π^- MWD or of a one-proton induced NMWD of ${}^{12}_{\Lambda}$B the vertex will be detected with good spatial resolution by the crossing of the tracks due to the three involved charged particles. The π^- from the MWD and the proton from NMWD will be detected by the range scintillator hodoscope. The excellent particle identification properties of the device will provide many independent measurements of the dE/dx of the charged particles traversing it. It should make possible the selection of protons from NMWD with an efficiency of about 99%. Indeed, for p-shell hypernuclei the proton induced NMWD width, recently determined experimentally [56], is larger than Γ_{π^-} by a factor from 2 to 5 depending on A.

As discussed in previous Sections, the range scintillator hodoscope will provide also the energy spectrum of the MWD π^- with a resolution of about 2 MeV (FWHM). Unfortunately, to our knowledge there are no predictions of such a spectrum. It must end at $\approx$ 116.5 MeV/c and experimentally should be very clean. We do not expect contaminations due to Λ_{free} decays, since B_Λ $\sim$11 MeV for $^{12}_{\Lambda}$B, and the selection on the MM will be very effective. Also the spectrum of protons from NMWD would be very clean. The contribution due to one-proton induced NMWD, needed to evaluate Γ_p, will be determined by the analysis of the upper part of the energy spectrum, following the procedure recently adopted in Ref. [58].

As far as the event numbers are concerned, we use the same approach as in Section 8, to obtain about 4×10^3 $^{12}_{\Lambda}$B hypernuclei with 5×10^{12} π^-'s on the ^{12}C targets. By means of the predicted value for Γ_{π^-}, about 7×10^2 events for the π^- decay should be obtained. About 1×10^3 protons from one-proton induced NMWD are expected, following the general trend of Γ_p for p-shell hypernuclei [58]. Then, thousands of events will be contained in the time delay spectra, allowing the determination of the lifetime of $^{12}_{\Lambda}$B, which has never been measured before, with a precision of better than 3%.

This layout is fully suited for measuring the observables τ, Γ_{π^-} and Γ_p for other mirror hypernuclei which can be obtained by using the (π^-, K^0) reaction on solid targets of ^{6}Li, ^{7}Li, ^{9}Be and ^{16}O (water in a thin-walled container), isotopically pure and easily assembled to form the tiles of the Venetian blind arrangement sketched by Fig. 16.

We do not expect that the Venetian blind geometry of the targets, which is not cylindrically symmetric, should introduce significant errors in the final values of the observables. Present reconstruction codes which will be used in the analysis can correct for the effects due to non-symmetric geometrical layouts. We recall that the precise values of τ, Γ_{π^-}, Γ_{π^0} and Γ_p for $^{12}_{\Lambda}$C were already obtained with a tilted target geometry [59].

As mentioned in Ref. [26], some minor modifications to the setup, namely the insertion of a suitably shaped thin Pb converter, could eventually permit the determination of Γ_{π^0} too. This way the full pattern of the partial WD widths should be obtained. As a matter of fact $\Gamma_{2\mathcal{N}}$ is well parameterized [58] and Γ_n may be obtained by difference. However, this feature must be examined carefully with a dedicated simulation.

B Possible determination of the Nonmesonic Weak decay width Γ_p for ${}^{3}_{\Lambda}$H and ${}^{4}_{\Lambda}$H hypernuclei

There are no experimental data on Γ_p for the Hydrogen hyperisotopes. We recall that among NMWD partial widths Γ_p, Γ_n, $\Gamma_{2\mathcal{N}}$, the first one is certainly the easier to be measured. On the other side the knowledge of $\Gamma_p({}^{4}_{\Lambda}\mathrm{H})$ is crucial for a clear assessment of the validity of the $\Delta\mathrm{I} = 1/2$ rule. We recall that the $\Delta\mathrm{I} = 1/2$ isospin rule was established empirically following the analysis of several non-leptonic strangeness changing processes, namely the K, Λ and Σ decays in free space. It is well established phenomenologically, but it is still unknown whether the large suppression of the $\mathrm{I} = 3/2$ amplitudes with respect to the $\mathrm{I} = 1/2$ ones holds as a general feature of all non-leptonic weak processes. A possible relevance of $\Delta\mathrm{I} = 3/2$ terms in hypernuclear NMWD would represent the first evidence for a $\Delta\mathrm{I} = 1/2$ rule violation in non-leptonic strangeness changing interactions. We remark that the $\Lambda N \to nN$ process has an important short-range part due to the higher momentum transfer, not accessible to non-leptonic strangeness changing decays of free $S = -1$ particles which follow the $\Delta\mathrm{I} = 1/2$ rule. Indeed, while the MWD involves only the $\Lambda N\pi$ vertex, which in free space obeys the $\Delta\mathrm{I} = 1/2$ rule, the NMWD involves also mesons heavier than the pion in the Λ vertex, through weak interaction couplings not available to the free decays. Nowadays, no experimental indication supports nor excludes the validity of the $\Delta\mathrm{I} = 1/2$ rule for these couplings and indirect information could come from hypernuclear NMWD. Moreover, it has been suggested that several weak $\Lambda N \to NN$ amplitudes are dominated by direct-quark processes in which no intermediate meson is involved [60, 61]. Such direct processes may not obey the $\Delta\mathrm{I} = 1/2$ rule.

To exploit at best this important option of really using hypernuclei as a laboratory to study interactions not otherwise allowed in free space it is useful to select simple systems, like the s-shell hyperisotopes of H and He (${}^{3}_{\Lambda}$H, ${}^{4}_{\Lambda}$H, ${}^{4}_{\Lambda}$He, ${}^{5}_{\Lambda}$He). For them the ΛN initial system is in the $\mathrm{L} = 0$ relative angular momentum state and it is possible to use the simple phenomenological model of Block-Dalitz [62]. Such an approach allows one to easily extract information on the spin-isospin dependence of the $\Lambda N \to nN$ process directly from data on s-shell hypernuclei. For them the neutron- and proton-induced decay widths are obtained in terms of a few spin- and isospin-dependent rates for the elementary process $\Lambda N \to nN$. The relationship among the elementary rates is strongly affected by the isospin change experienced in the NMWD, both $\Delta\mathrm{I} = 1/2$ and $\Delta\mathrm{I} = 3/2$ being in principle possible.

A first attempt to verify the validity of the $\Delta I = 1/2$ rule by using the existing, poor quality, data on various NMWD exclusive channels of s-shell hypernuclei was performed in Ref. [63]. A suggestion that a large violation of the $\Delta I = 1/2$ rule could be observed in NMWD of s-shell hypernuclei was put forward. However, due to the large errors affecting the experimental data that were considered, ranging from 38% to 59%, the result could not be considered as definitive. As a matter of fact, an analysis of more recent experimental data, performed in Ref. [64] always with the phenomenological Block-Dalitz model, reinforced the previous doubts. It was concluded that the large error bars do not allow to draw definitive conclusions about the possible violation of the $\Delta I = 1/2$ rule and the spin dependence of the Block-Dalitz transition rates. The data turned out to be consistent with the hypothesis of validity of the $\Delta I = 1/2$ rule at the level of 60%. In other words, the $\Delta I = 1/2$ rule could be excluded only at the 40% confidence level. This result is not changed much if some present data, more precise, are used.

Among the different equalities and inequalities concerning exclusive NMWD channels which can be obtained in the limit of pure $\Delta I = 1/2$ transitions the most interesting one, from a theoretical point of view, looks to be $\Gamma_n(^4_\Lambda\mathrm{He})/\Gamma_p(^4_\Lambda\mathrm{H})$ which should be equal to 2. It should be equal to 1/2 for a pure $\Delta I = 3/2$ transition. For Γ_n/Γ_T of $^4_\Lambda$He only an upper limit of 0.032 (at 95% C.L.) exists [65]. The approved experiment E22 at J-PARC aims to a determination of such a value. Taking into account the number previously quoted for the MWD of $^4_\Lambda$H (1.5×10^3 events for the π^- WD, with a B.R. of 49%) we may expect ≈ 15 decays for the proton-induced WD at the 1% B.R.. This decay channel should be visible as a broad peak in the proton spectrum, centered around 80 MeV and about 15 MeV wide, due to the kinematic of the $\Lambda p \to np$ weak reaction in $^4_\Lambda$H, broadened by the Fermi motion. No substantial Final State Interaction (FSI) effects are expected as well as no contribution for the $2\mathcal{N}$-induced NMWD, as shown by the clean spectrum obtained for the mirror system $^4_\Lambda$He [65, 66].

References

[1] D.H. Davis, Nucl. Phys. A 754 (2005) 3.

[2] H. Kamada, J. Golak, K. Miyagawa, H. Witala, W. Glockle, Phys. Rev. C 57 (1998) 1595.

[3] M. Tanabashi *et al.* (Particle Data Group), Phys. Rev. D 98 (2018) 030001.

[4] O. Hashimoto, T. Tamura, Progr. Part. Nucl. Phys. 57 (2006) 564.

[5] T. Bressani in Proc. of Int. School of Physics "Enrico Fermi" Course CLXVII, edited by M. Anselmino, T. Bressani, A. Feliciello, Ph.G. Ratcliffe (SIF, Bologna and IOS Press, Amsterdam, 2008), p.3.

[6] E. Botta, T. Bressani, G. Garbarino, Eur. Phys. J. A (2012), 48:41.

[7] A. Feliciello, T Nagae, Rept. Prog. Phys. 78 (2015) 096301.

[8] E. Botta, T. Bressani, S. Bufalino A. Feliciello, Riv. N. Cim. 38 (2015) 387.

[9] M. M. Block *et al.*, Proc. of Int. Conf. on Hyperfragments, St. Cergue, Switzerland, 28-30 March 1963, p. 63.

[10] F. Schulz *et al.* (A1 Collaboration), Nucl. Phys. A 954 (2016) 149.

[11] R.J. Prem and P.H. Steinberg, Phys. Rev. 136 (1964) B1803.

[12] Y.V. Kang *et al.*, Phys. Rev. 139 (1965) B401.

[13] G. Keyes *et al.*, Phys. Rev. Lett. 20 (1968) 819.

[14] R. J. Phillips and J. Schneps, Phys. Rev. Lett. 20 (1968) 1383.

[15] R. J. Phillips and J. Schneps, Phys. Rev. 180 (1969) 1307.

[16] G. Bohm *et al.*, Nucl. Phys. B 16 (1970) 46.

[17] G. Keyes *et al.*, Phys. Rev. D 1 (1970) 66.

[18] G. Keyes *et al.*, Nucl. Phys. B 67 (1973) 269.

[19] S. Avramenko *et al.*, Nucl. Phys. A 547 (1992) 95c.

[20] STAR Collaboration, Science 328 (2010) 58.

[21] Y. Zhu, Nucl. Phys. A 904 (2013) 551c.

[22] C. Rappold *et al.*, Nucl. Phys. A 913 (2013) 170.

[23] ALICE Collaboration, J. Adam *et al.*, Phys. Lett. B 754 (2016) 360.

[24] STAR Collaboration, Nucl. Phys. A 904 (2013) 551c.

[25] STAR Collaboration, Phys, Rev. C 97 (2018) 054909.

[26] A. Agnello, E. Botta, T. Bressani, S. Bufalino, A. Feliciello, Nucl. Phys. A 954 (2016) 176.

[27] R. Barlow, arXiv.0406.120 (2004)

[28] N. Crayton *et al.*, Proc. 11th Int. Conf. on High Energy Physics, CERN (1962) p. 460

[29] J.J. Szymanski *et al.*, Phys. Rev. C 43 (1991) 849.

[30] H. Outa *et al.*, Nucl. Phys. A 585 (1995) 109c.

[31] A. Dainese *et al.*, "INFN What Next: Ultra-relativistic Heavy-Ion Collisions", arXiv:1602.04120.

[32] M. Rayet, R.H. Dalitz, Il Nuovo Cim. A 46 (1966) 786.

[33] M. Ram, W. Williams, Nucl. Phys. B 28 (1971) 566.

[34] H. Mansour, K. Higgins, Il Nuovo Cim. A 51 (1979) 180.

[35] N. Kolesnikov, V. Kopylov, Sov. Phys. J. 31 (1988) 210.

[36] J.G. Congleton, J. Phys. G, Nucl. Part. Phys. 18 (1992) 339.

[37] F. Dohrmann *et al.*, Phys. Rev. Lett. 93 (2004) 242501

[38] F. Garibaldi *et al.*, JLab proposal (R12-15-008)2015, `https://www.jlab.org/expprog/proposals/15prop.html`.

[39] E. Botta, JPS Conf. Proc. 17 (2017) 021006.

[40] Y. Akazawa *et al.*, J-PARC proposal P63 (2016), `http://j-parc.jp/researcher/Hadron/en/Proposal.e.html`.

[41] H. Hotchi *et al.*, Phys. Rev. C 64 (2001) 044302.

[42] GEANT4 Collaboration, Nucl. Instr. Meth. A 506 (2003) 250.

[43] J.F. Ziegler *et al.*, Nucl. Instr. Meth. B 268 (2010) 1818.

[44] T. Takahashi *et al.*, Prog. Theor. Exp. Phys. 2012, 02B010.

[45] H. Park *et al.*, Phys. Rev. C 61 (2000) 054004.

[46] G.C. Bonazzola *et al.*, IEEE Trans. Nucl. Sci. NS-38 (2) (1991) 393.

[47] T. Harada, private communication (2006).

[48] H. Tamura *et al.*, Phys. Rev. C 40 (1989) R479.

[49] R.J. Peterson, Few-Body Syst. Suppl. 9 (1995) 17.

[50] A.S. Clough *et al.*, Nucl. Phys. B 76 (1974) 15.

[51] S. Ajimura *et al.*, J-PARC proposal P22 (2006), `http://j-parc.jp/researcher/Hadron/en/Proposal.e.html`.

[52] K. Itonaga, T. Motoba, Prog. Theor. Phys. Suppl. 185 (2010) 252.

[53] M. Agnello *et al.* (FINUDA Collaboration and A. Gal), Phys. Lett. B 681 (2009) 139.

[54] R.H. Dalitz, Phys. Rev. 112 (1958) 605.

[55] D. Cohen, S. Kurath, Nucl. Phys. 73 (1965) 1.

[56] E. Botta, T. Bressani, S. Bufalino, A. Feliciello, Phys. Lett. B 748 (2015) 86.

[57] Y. Sato *et al.*, Phys. Rev. C 71 (2005) 025203.

[58] M. Agnello *et al.* (FINUDA Collaboration), Phys. Lett. B 738 (2014) 499.

[59] H. Bhang, *et al.*, J. Korean Phys. Soc. 59 (2011) 1461.

[60] T. Inoue, M. Oka, T. Motoba, K. Itonaga, Nucl. Phys. A 633 (1998) 312.

[61] K. Sasaki, M.Izaki, M. Oka, Phys. Rev. C 71 (2005) 035502.

[62] M.M. Block, R.H. Dalitz, Phys. Rev. Lett. 11 (1963) 96.

[63] R. Schumacher *et al.*, Nucl. Phys. A 547 (1992) 143.

[64] W.M. Alberico, G. Garbarino, Phys. Lett. B 486 (2000) 362.

[65] J.D. Parker *et al.*, Phys. Rev. C 76 (2007) 035501.

[66] H. Outa *et al.*, Nucl. Phys. A 639 (1998) 251c.